EXTRA SPINDLE POLES (Separase) controls anisotropic cell expansion in Norway spruce (Picea abies) embryos independently of its role in anaphase progression

Panagiotis N. Moschou[1], Eugene I. Savenkov[1*], Elena A. Minina[1,2*], Kazutake Fukada[1*], Salim Hossain Reza[1,2], Emilio Gutierrez-Beltran[1,2], Victoria Sanchez-Vera[1], Maria F. Suarez[3], Patrick J. Hussey[4], Andrei P. Smertenko[5,6] and Peter V. Bozhkov[1,2]

1. Department of Plant Biology, Uppsala BioCenter, Swedish University of Agricultural Sciences and Linnean Center for Plant Biology, PO Box 7080, SE-75007 Uppsala, Sweden;

2. Department of Chemistry and Biotechnology, Uppsala BioCenter, Swedish University of Agricultural Sciences and Linnean Center for Plant Biology, PO Box 7015, SE-75007 Uppsala, Sweden;

3. Departamento de Biologia Molecular y Bioquimica, Facultad de Ciencias, Universidad de Malaga, 290071 Malaga, Spain;

4 .The Integrative Cell Biology Laboratory, School of Biological and Biomedical Sciences, University of Durham, Durham, DH1 3LE, UK;

5. Institute of Biological Chemistry, Washington State University, Pullman, WA 99164, USA;

6. Institute for Global Food Security, Queen's University Belfast, 18–30 Malone Road, Belfast, BT9 5BN, UK

*These authors contributed equally to this work.

Author for correspondence:Panagiotis N. Moschou

Tel: +46 700780553

Email: panagiotis.moschou@slu.se

Received: 29 February 2016

Accepted: 7 April 2016

New Phytologist (2016) 212: 232–243

doi: 10.1111/nph.14012

Key words: cell cycle, embryogenesis, microtubules, proteases, separase, spruce (Picea abies).

Summary

- The caspase-related protease separase (EXTRA SPINDLE POLES, ESP) plays a major role in chromatid disjunction and cell expansion in Arabidopsis thaliana. Whether the expansion phenotypes are linked to defects in cell division in Arabidopsis ESP mutants remains elusive. Here we present the identification, cloning and characterization of the gymnosperm Nor-way spruce (Picea abies, Pa) ESP. We used the P. abies somatic embryo system and a combi-nation of reverse genetics and microscopy to explore the roles of Pa ESP during embryogenesis.
- Pa ESP was expressed in the proliferating embryonal mass, while it was absent in the sus-pensor cells. Pa ESP associated with kinetochore microtubules in metaphase and then with anaphase spindle midzone. During cytokinesis, it localized on the phragmoplast microtubules and on the cell plate. Pa ESP deficiency perturbed anisotropic expansion and reduced mitotic divisions in cotyledonary embryos. Furthermore, whilst Pa ESP can rescue the chromatid nondisjunction phenotype of Arabidopsis ESP mutants, it cannot rescue anisotropic cell expansion.
- Our data demonstrate that the roles of ESP in daughter chromatid separation and cell expansion are conserved between gymnosperms and angiosperms. However, the mechanisms of ESP-mediated regulation of cell expansion seem to be lineage-specific.

Introduction

Embryonic pattern formation in seed plants involves the estab-lishment of apical–basal and radial polarities resulting in the for-mation of primary shoot and root meristems (Mayer et al., 1991; Meinke, 1991; Ueda & Laux, 2012). Knowledge about plant embryogenesis has benefited from studies of embryo-defective mutants in the angiosperm model species Arabidopsis thaliana (Mayer et al., 1991; Capron et al., 2009; Kanei et al., 2012; Wendrich & Weijers, 2013). However, our understanding of the molecular mechanisms underlying embryogenesis remains lim-ited, owing to the restricted accessibility of zygotic embryos dur-ing early developmental stages. Somatic embryogenesis represents a valuable model for studying regulation of embryogenesis, as it allows synchronized production of a large number of embryos at a specific developmental stage and their life imaging (Pennell et al., 1992; von Arnold et al., 2002; Smertenko & Bozhkov, 2014).

Early embryogenesis in Arabidopsis proceeds through highly regular cell division patterns, starting with an asymmetric first division of the zygote, which gives rise to a smaller apical and a larger basal cell. The basal cell divides transversely to form a sin-gle file of suspensor cells and a hypophysis cell, while the apical cell undergoes several rounds of divisions to give rise to a globular embryo. This stage is followed by the establishment of bilateral symmetry and differentiation of two cotyledons. In most gym-nosperms (e.g. Norway spruce, Picea abies), the zygote undergoes several rounds of karyokinesis without cytokinesis (free nuclear stage), followed by cellularization and formation of the lowest and the upper cell tiers (Singh, 1978). The lowest tier will form the embryonal mass (gymnosperm equivalent of embryo proper), while the upper tier will form the first layer of suspensor. A fully developed suspensor in spruce embryos is composed of several layers of nondividing elongating cells. Unlike Arabidopsis embryos, spruce embryos form a crown of multiple cotyledons with radial symmetry surrounding the shoot apical meristem (Singh, 1978). Despite morphological differences in the embryo patterning in different plant lineages, the core regulatory network appears to be conserved (reviewed in Smertenko & Bozhkov, 2014).

Previous studies highlighted the importance of proteases in plant embryogenesis and other developmental processes (van der Hoorn, 2008). For example, in Arabidopsis the subtilisin-

like serine protease ALE1 is required for cuticle formation in protoderm (Tanaka et al., 2001) and the phytocalpain DEK1 is essential for embryogenic cell fate determination (Johnson et al., 2005). DEK1 mutant embryos that develop beyond glob-ular stage show aberrant cell division planes in the suspensor and embryo proper (Johnson et al., 2005; Lid et al., 2005). In addition, early embryonic patterning in Norway spruce requires the activity of metacaspase mcII-Pa (Suarez et al., 2004; Minina et al., 2013). Knockdown of mcII-Pa suppresses differentiation of the suspensor and abrogates establishment of apical–basal polarity.

Separase (Extra Spindle Poles, ESP) is a caspase-related pro-tease indispensable for embryogenesis in Arabidopsis (Liu & Makaroff, 2006) and nonplant species (e.g. Bembenek et al., 2010). Initially, ESP was identified as an evolutionary con-served protein that cleaves cohesin to enable disjunction of sis-ter chromatids during metaphase-to-anaphase transition (referred to as the canonical function of ESP; Ciosk et al., 1998). A temperature-sensitive mutant allele of ESP from Arabidopsis (At ESP), rsw4 (radially swollen 4), exhibits a chro-mosome nondisjunction phenotype (Wu et al., 2010). In addi-tion, rsw4 causes disorganization of the radial microtubule system in meiocytes (Yang et al., 2011) and defects in anisotropic expansion of root cells associated with radial swelling (Wu et al., 2010).

Previously, we examined the role of At ESP in cell polarity and found that At ESP controls microtubule-dependent trafficking that is essential for cell plate synthesis during cytokinesis (Moschou et al., 2013). Here we report on the identification and functional characterization of the gymnosperm Norway spruce (P. abies) ESP homologue Pa ESP, and explore the phenotype of spruce embryos depleted of Pa ESP.

Materials and Methods

Plant material and growth conditions

The Picea abies (L.) H. Karst. (Norway spruce) wild-type (WT) embryogenic cell lines 95.88.22 and 95.61.21, and Pa ESP-RNAi lines were cultured as described previously (Filonova et al., 2000). Embryonal masses were separated from the suspensors of 7-d-old embryos using surgical blades in droplets of culture medium under a binocular microscope.

Molecular biology

Primers used in this study are listed in Supporting Informa-tion Table S1. Full-length cDNA of the Pa ESP was obtained by 50- and 30-rapid amplification of cDNA ends (RACE) with the SMART RACE cDNA Amplification kit (Clontech, Mountain View, CA, USA) and Advantage 2 PCR kit (Clontech), with primers designed from publicly available sequences of expression sequence tags (http://congenie.org/). Amplified PCR products were cloned into pCR4Blunt-Topo (Invitrogen, Carlsbad, CA, USA). The plasmid-carrying FLAG-PaESP sequence was con-structed by ligating a 50-FLAG-PaESP fragment digested with PacI and AatII with the 30-end fragment digested with AatII and Sse8783I into the PacI/Sse8783I-cleaved vector pAHC25.

The FLAG-PaESP plasmid was used as a template to amplify by PCR two overlapping fragments using the primers FWPaESPExp1topo-Se-R3 (50-fragment) and RvPaESPEXPAscI-Se-F2 (30-fragment). The overlapping region contained a ClaI restriction site. The 50-fragment was introduced into the pTOPO/D vector (Invitrogen) giving rise to the pTOPO/D-PaESP 3.0 kb. The pTOPO/D vector contains an AscI site, upstream of the attR2

site. The remaining part of Pa ESP was introduced by digesting the 30-fragment by ClaIandAscI and ligating it into pTOPO/D-PaESP 3.0 kb digested with ClaI and AscI, thus producing pTOPO/D-PaESP 6.9 kb. The Pa ESP insert was sub-cloned into the pGWB15 (39HA-tagged) vector by the gateway recombination reaction using the LR enzyme (Invitrogen).

A 2423-bp-long C-terminal fragment was amplified with primers Sep-C-terminus CHis-P, Sep-CHis-M1 and Sep-CHis-M2 from pTOPO/D-PaESP 6.9 kb and introduced into a modi-fied pET11a vector (Qiagen, Valencia, CA, USA). The pET11a vector was modified by introducing a part from the polylinker of pKOH122 digested with NdeIandBamHI (amplified by pKOH122-MCS-P and MCS-reverse-with-SacI).

For constructing the Pa ESP-RNAi vector, two fragments were amplified using the primers FWPaESPExp1topo, PaESPRN-AiRV1EcoRI and FwPaESPRNAiAscI, PaESPRNAiRV2EcoRI. Primer PaESPRNAiRV2EcoRI anneals 400 bp downstream of the PaESPRNAiRV1EcoRI. This 400 bp region represents the loop between two arms of the hairpin. The first fragment was cloned in a pTOPO/D vector, which was subsequently digested with EcoRI and AscI and the second fragment was introduced by ligation producing the pTOPO/D-hpRNAiPaESP vector. The hairpin insert was subcloned into a pGWB2 vector (constitutive silencing; Nakagawa et al., 2007) or the pMDC7 (LexA-VP16-ER (XVE) b-estradiol-inducible promoter, which is derived from the pER8 vector and contains the oestrogen receptor-based trans-activator XVE; Brand et al., 2006). The resulting constructs, pGWB2-hpRNAiPaESP and pMDC7-hpRNAiPaESP, were transformed into Agrobacterium tumefaciens GV3101 by electro-poration. All constructs were verified by sequencing.

Phylogenetic analysis

Alignments of ESP sequences were performed in CLUSTALW. Unrooted trees were constructed using the neighbour-joining method (Saitou & Nei, 1987) using the yeast homologue as an outgroup. A phylodendrogram was constructed using PAUP soft-ware (http://paup.csit.fsu.edu). The bootstrap analysis was per-formed with 2000 repeats, and branches with bootstrap values over 70% were retained.

Embryo transformation and transient expression

Norway spruce embryogenic cultures were transformed by A. tumefaciens GV3101. Agrobacteria were grown overnight in Luria-Bertani (LB) medium supplemented with 10 mM $MgCl_2$, 10 mM 2-(N-morpholino)ethane sulfonic acid (MES), pH 5.5, 40 μM acetosyringone, 50 μg ml^{-1} rifampicin and 50 μg ml^{-1} kanamycin. Agrobacteria were collected and incubated for 1 h in 10 mM $MgCl_2$, 10 mM MES, pH 5.5, and 150 μM acetosyringone at room temperature on a shaker (OD600 = 10). Ten microlitres of 5-d-old spruce culture (cell line 95.88.22) were collected in a 50 ml tube and the supernatant was discarded. The spruce culture was coincubated with 1 ml Agrobacterium in 10 ml of 10 mM $MgCl_2$, 10 mM MES, pH 5.5, and 150 μM acetosyringone for 8 h without shaking at 20°C in darkness. Excess liquid was removed and spruce cells were placed on three layers of sterile filter paper. The upper layer was transferred onto half-strength Le Poivre (LP) medium (Filonova et al., 2008). After 48 h, filter paper was transferred onto half-strength LP medium supplemented with 250 μg ml^{-1} cefotaxime (Duchefa, Haarlem, the Netherlands), and, after an additional 7 d, onto the same medium containing 15 μg ml^{-1} hygromycin B (Duchefa). Filters were transferred onto fresh medium once a week for 6 wk consecutively. Subsequently, cell colonies were transferred onto

the medium without filter papers, and grown in the presence of 250 μg ml^{-1} cefotaxime, 400 μg ml^{-1} timentin (Duchefa) and 15 μg ml^{-1} hygromycin B. After colonies were grown to c.2cm in diameter, suspension cultures were established in half-strength LP without selection agents.

For transient expression of Pa ESP-RNAi, Norway spruce embryogenic cultures were transformed by A. tumefaciens as described earlier with minor modifications. The cell line 95.61.21 was used and, after cefotaxime treatment for 2 d, cells were fixed and stained with 40,6-diamidino-2-phenylindole (DAPI). As a control, a pMDC32 vector containing the cDNA encoding for monomeric red fluorescent protein (mRFP) was used.

Absolute quantitative RT-PCR analyses

Quantitative real-time polymerase chain reaction (qRT-PCR) was done as previously described (Moschou et al., 2013). For absolute quantification of cDNA molecules in the qRT-PCR, At ESP or Pa ESP in pGWB15 vectors were used as standards.

Preparation of immunogen and antibody

The pET11a-PaESP construct was transformed in BL21-CodonPlus (DE3) RIL (Stratagene, La Jolla, CA, USA) Escherichia coli competent cells. Purification of the His-tagged recombinant C-terminal fragment containing the C50 domain (1502–2307 amino acids (aa)) of Pa ESP was performed according to manufac-turer's instructions (Qiagen). Antisera were raised in three mice.

Western blot analysis

A quantity of 100 mg of plant material was mixed with 200 llof 2 9 Laemmli sample buffer (Laemmli, 1970), kept on ice for 10 min and boiled for 5 min. Samples were centrifuged at 17 000 g for 15 min. Equal amounts of each supernatant were loaded on 9% or 4–15% gradient polyacrylamide gels and blot-ted on a polyvinylidene fluoride membrane (see also Methods S1). Anti-Pa ESP and anti-actin C4 were used at dilutions of 1 : 1000 and 1 : 200, respectively; anti-mouse horseradish peroxi-dase conjugates (GE Healthcare, Uppsala, Sweden) were used at a dilution 1 : 5000. Blots were developed using the ECL Prime kit (GE Healthcare) and imaged in a LAS-3000 Luminescent Image Analyzer (Fujifilm, Fuji Photo Film, Kleve, Germany).

Immunocytochemistry and imaging

The immunostaining of embryos was performed using a previ-ously established protocol (Smertenko & Hussey, 2008). Two-day-old early embryos of Norway spruce were fixed in 3.7%(w/v) formaldehyde in microtubule-stabilizing buffer (MTSB; 0.1 M piperazine-N,N0-bis(2-ethane sulfonic acid) (PIPES), pH 6.8, 5 mM EGTA, 2 mM $MgCl_2$) supplemented with 1%(v/v) Triton X-100. For methanol fixation, cells were fixed in strainers with 100% (v/v) methanol for 10 min at -20°C, followed by 100% (v/v) acetone for 5 min at -20°C. The cells were then washed three times for 5 min each with phosphate-buffered saline (PBS) at room temperature and allowed to rehydrate in PBS for additional 30 min at room temperature before treatment with cell wall-digesting enzymes. Embryos were blocked with PBS Tween-20 (PBST) supplemented with 5% (w/v) BSA (blocking solution). Subsequently, embryos were incubated overnight with rabbit anti-Pa ESP, diluted 1 : 500, and rat anti-tubulin YL1/2 (AbD Serotec, Oxford, UK), diluted 1 : 200 in blocking solution. Specimens were then washed three

times for 30 min in PBST and incubated for 3 h with goat anti-rat TRITC (tetramethyl rhodamine isothiocyanate) and anti-rabbit FITC (fluorescein isothio-cyanate conjugated) secondary antibodies diluted 1 : 200 in blocking solution. After washing in PBST, specimens were mounted in Vectashield (Vector Laboratories, Burlingame, CA, USA) mounting medium. The samples were examined using a Leica SP5 or Zeiss 710 confocal microscope equipped with oil immersion (963 with numerical aperture = 1.4) objective.

Tissue sectioning

Cotyledonary embryos were fixed for 2 h at room temperature under vacuum with 4% (w/v) paraformaldehyde in MTSB sup-plemented with 0.4% (v/v) Triton X-100. The fixative was washed away with PBST buffer, and embryos were dehydrated on ice by 0.85% (w/v) NaCl (30 min) and an ethanol (EtOH) gradient in 0.85% (w/v) NaCl (50%, 70%, 85%, 95% and 100% for 90 min each, 100% overnight and 100% for 2 h). Sam-ples were treated twice with 100% (v/v) xylene at room tempera-ture for 1 h each, overnight with 50% (v/v) xylene supplemented with 50% (w/v) histowax at 40–50°C, and 100% (w/v) histowax at 60°C, changing twice per day for 3 d consecutively. Samples were stored at 4°C until they were used. Sections of 10 lm thick-ness were cut using a microtome and placed on poly-lysine-coated slides in water droplets. Water was allowed to evaporate overnight at 45°C. Samples were deparaffinized and rehy-drated by two washes, 10 min each, in histoclear, two washes, 2 min each, in 100% (v/v) EtOH, followed by an EtOH gradient (95%, 90%, 80%, 60% and 30%) in PBS for 2 min for each step. Slides were treated for 2 min with H2O and 20 min with PBS. Sections were blocked and hybridized with antibodies as described earlier.

Microtubule and image analysis

The image and pixel analyses were done using IMAGEJ v.1.48 soft-ware (http://rsb.info.nih.gov/ij). Intensity profile was calculated along an interactively applied line, and data of intensity measure-ments were exported to Microsoft EXCEL (Microsoft, Redmond, WA, USA) and plotted. Default modules and options were used. Images were prepared using Adobe PHOTOSHOP CS6 (Adobe, San Jose, CA, USA).

Statistical analysis

Graphs were prepared using EXCEL v.2013 or JMP v.11 (Division of SAS, Cary, NC, USA). Statistical analysis was performed with JMP v.11. Statistical methods used are indicated in the corre-sponding figure legends.

Results

Identification, cloning and sequence analysis of Pa ESP

All known ESP proteins are encoded by single genes, with the sole exception of Drosophila melanogaster ESP, which contains two subunits encoded by separate genes (reviewed in Moschou & Bozhkov, 2012). The full-length cDNA for Pa ESP was isolated by RACE, using internal primers that spanned the conserved 30-end of the gene (Notes S1, S2). The cDNA was sequenced and found to be 7248 bp long and contained an open reading frame encoding a

polypeptide of 2308 aa with predicted molecular mass of 259 kDa. We deposited the Pa ESP sequence in GenBank under the accession number HE793991.1. Phylogenetic analysis revealed that Pa ESP together with the ESP homologue from Pinus taeda form one clade with mosses, which locates between Klebsormidium and angiosperms (Fig. 1a; Notes S1). The C-terminus of Pa ESP contains a conserved caspase-related prote-olytic domain (Pfam number PF03568; 1673–2187 aa, P = 7.1e^{-88}; Fig. 1b) with the His and Cys catalytic dyad typical for all members of CD-clan proteases (Aravind & Koonin, 2002). This proteolytic domain is the most conserved region of Pa ESP, showing 30% and 31% identity with the corresponding domains of human and budding yeast homologues, respectively, and over 50% identity with plant homologues. The rest of the sequence is less conserved, suggesting functional divergence of ESP proteins. In contrast to mammalian homologues, all plant ESP proteins lack a well-defined leucine-rich region, which may be responsible for DNA binding (Fig. 1c; Sun et al., 2009). Fur-thermore, Pa ESP lacks the Ca2+-binding EF-hand and 2Fe-2S motifs identified in the Arabidopsis homologue (Fig. 1c). These differences in the primary sequence combined with the mono-phyletic nature of the phylodendrogram suggest that ESP func-tions were fine-tuned in different lineages during evolution.

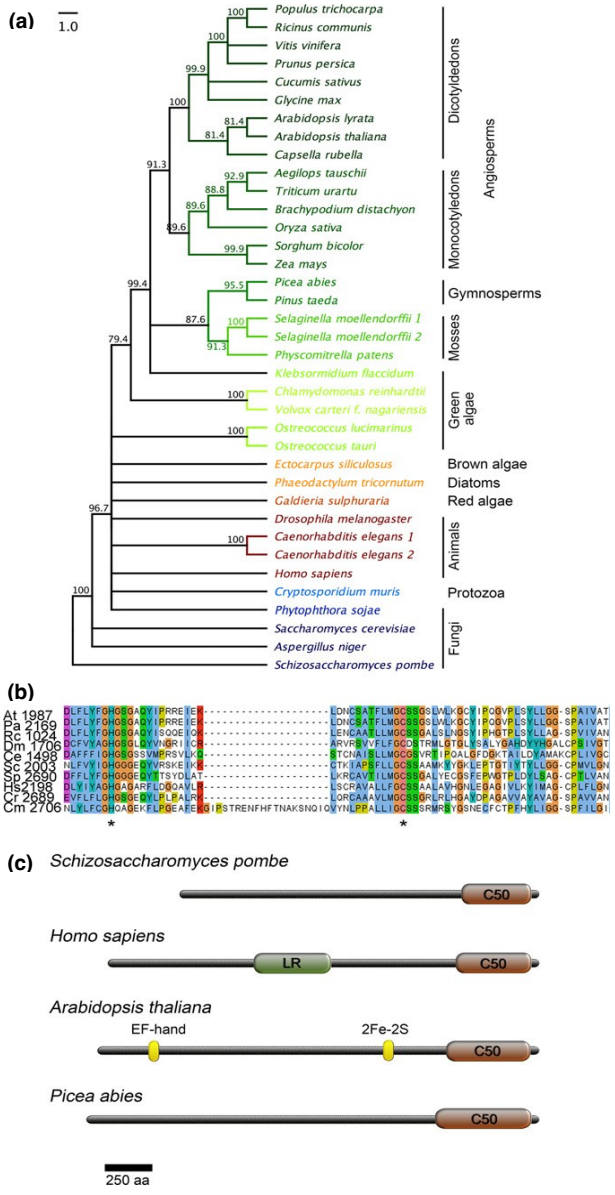

Fig. 1 Analysis of Picea abies EXTRA SPINDLE POLES (Pa ESP) sequence. (a) Phylodendrogram of ESP protein homologues. The Saccharomyces cerevisiae protein sequence was used as an outgroup. The bootstrap values are indicated at the branching points. Accession numbers are indicated in Supporting Information Notes S2. (b) Alignment of amino acid (aa) sequences corresponding to the C50 proteolytic domain of ESP proteins. At, Arabidopsis thaliana; Rc, Ricinus communis; Dm, Drosophila melanogaster; Sc, Saccharomyces cerevisiae; Ce, Caenorhabditis elegans; Sp, Schizosaccharomyces pombe; Hs, Homo sapiens; Cr, Cryptosporidium parvum; Cm, Chlamydomonas reinhardtii; Pa, Picea abies. Asterisks denote the conserved His, Cys dyad. Full alignment is shown in Notes S1.(c) Domain organization of selected ESP proteases. C50, proteolytic domain; LR, leucine-rich domain; EF-hand, helix–loop–helix topology with the ability to bind Ca2+; 2Fe-2S, iron-sulphur cluster.

Pa ESP protein abundance is developmentally regulated

Early somatic embryos of Norway spruce develop form unorga-nized multicellular aggregates called proembryogenic masses (PEMs) upon withdrawal of the plant growth regulators (PGRs) auxin and cytokinin (Fig. 2a). The later stages of somatic embryogenesis resemble those of the zygotic pathway and are promoted by abscisic acid (ABA; Filonova et al., 2000). An early spruce embryo is composed of the embryonal mass, tube cells and the suspensor (Fig. 2a). While the embry-onal mass gives rise to the mature embryo, the suspensor is a transient structure undergoing programmed cell death (Filonova et al., 2000). The suspensor cells in Norway spruce embryos are formed via asymmetric cell divisions in the basal-most part of the embryonal mass. Following asymmetric cell division, the upper daughter cell retains its meristematic iden-tity and remains within the embryonal mass, while its sister (lower) cell becomes a terminally differentiated tube cell. The tube cells cease proliferation and expand anisotropically to form suspensor cells. Addition of new tube cells through reiter-ated cell divisions in the embryonal mass creates long files composed of several suspensor cells at successive stages of pro-grammed cell death along the apical–basal axis. The hollow-walled corpses of suspensor cells are removed from the basal end of the embryo-suspensors (Bozhkov et al., 2005).

To analyse the levels of Pa ESP at successive stages of plant development, we raised an antibody against the C50 catalytic domain of Pa ESP and used it in immunoblotting. The antibody recognized a protein of c. 260 kDa that corresponds to the pre-dicted size of Pa ESP (Methods S1). Protein abundance of Pa ESP was high in proliferating PEMs in the presence of PGR (+PGR), but not during differentiation of early embryos (-PGR; Fig. 2b), and in the microsurgically separated embryonal masses of early embryos (Fig. 2c). Neither suspensor cells nor distinct parts of seedlings, including cotyledons, young needles, hypocotyls and roots, contained detectable amounts of Pa ESP protein, demonstrating that high amounts of Pa ESP are associ-ated with actively proliferating tissues. The amount of Pa ESP seems to be regulated at the transcriptional level, as suspensor cells, cotyledons, hypocotyls and roots contained at least five-fold less Pa ESP mRNA than the embryonal mass (Fig. S1a).

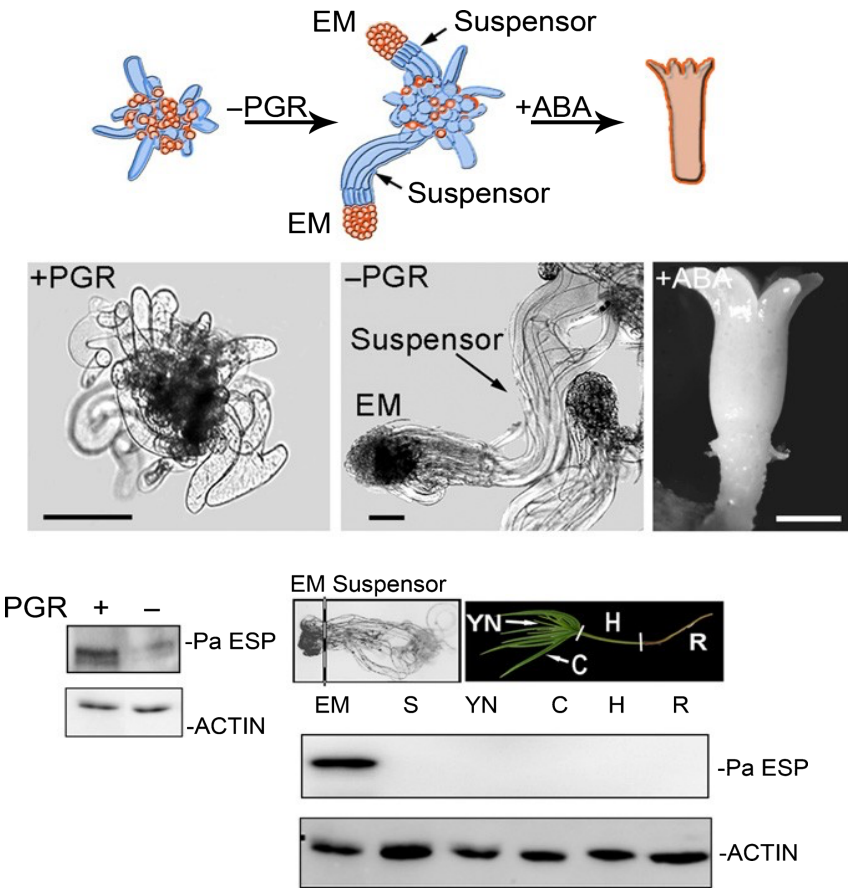

Fig. 2 Picea abies EXTRA SPINDLE POLES (Pa ESP) level is developmentally regulated. (a) A model (adapted from Filonova et al., 2000) and corresponding micrographs of three principal stages of Norway spruce somatic embryogenesis. Red and blue colours denote proliferating and dying cells, respectively. EM, embryonal mass; PGR, plant growth regulators; ABA, abscisic acid. Bars, 100 lm. (b) Western blot analysis of Pa ESP in 2-d-old embryogenic culture grown in the presence (+PGR) or absence (-PGR) of PGR. (c) Western blot analysis of Pa ESP in the embryonal masses (EM) and suspensors (S); on the Western blot) of early somatic embryos, as well as in cotyledons (C), young needles (YN), hypocotyls (H) and roots (R) of seedlings. The equal loading was confirmed using anti-actin. The images of representative plant material used for protein extraction are shown above the Western blot.

Pa ESP localizes to microtubules and associates with the cell plate during cytokinesis

The intracellular localization of Pa ESP in the meristematic cells of PEMs and early embryos was examined using immunofluores-cence microscopy (Figs 3, S2). In nondividing meristematic cells, Pa ESP decorated cortical microtubules (Fig. S2, top images), while during preprophase, Pa ESP was found on the preprophase band and perinuclear basket of microtubules (Fig. 3a,b1). At the beginning of prophase and until the onset of anaphase, Pa ESP was detected around the mitotic spindle, as well as on the kineto-chore microtubules (Fig. 3b2). At the onset of anaphase, most Pa ESP was associated with the spindle poles and midzone micro-tubules (Fig. 3b3,c). This localization was independent of the fix-ation method as the same staining pattern was observed after more stringent fixation with methanol/acetone, which exposes epitopes masked by protein folding or interaction with other pro-teins (Fig. 3c). Densitometry profiling of the anaphase spindle revealed three apparent peaks corresponding to both spindle poles and the midzone (Fig. 3c). During telophase, Pa ESP con-centrated in the phragmoplast midzone, where the cell plate is assembled (Fig. 3b4). A similar localization was observed after the methanol/acetone fixation and the densitometry profiling revealed only one major peak of fluorescence in the phragmoplast midzone (Fig. 3d). Apart from the midzone, Pa

ESP colocalized with microtubules at the leading edge of the phragmoplast in all cases examined (n = 53; Fig. 3b4, inset). At later stages of phrag-moplast development, Pa ESP remained at the cell plate after the depolymerization of microtubules (Fig. 3b5).

We examined localization of Pa ESP in the first layer of anisotropically expanding cells adjacent to the embryonal mass, the tube cells. These cells cease proliferation, becoming commit-ted to programmed cell death. During the subsequent differentia-tion steps, the tube cells elongate to form stereotypical suspensor cells (Bozhkov et al., 2005; Smertenko & Bozhkov, 2014; Zhu et al., 2014). Pa ESP was absent from these cells (Fig. S2, lower images), consistent with the finding that the Pa ESP mRNA level is greatly reduced in the suspensor (Fig. S1a).

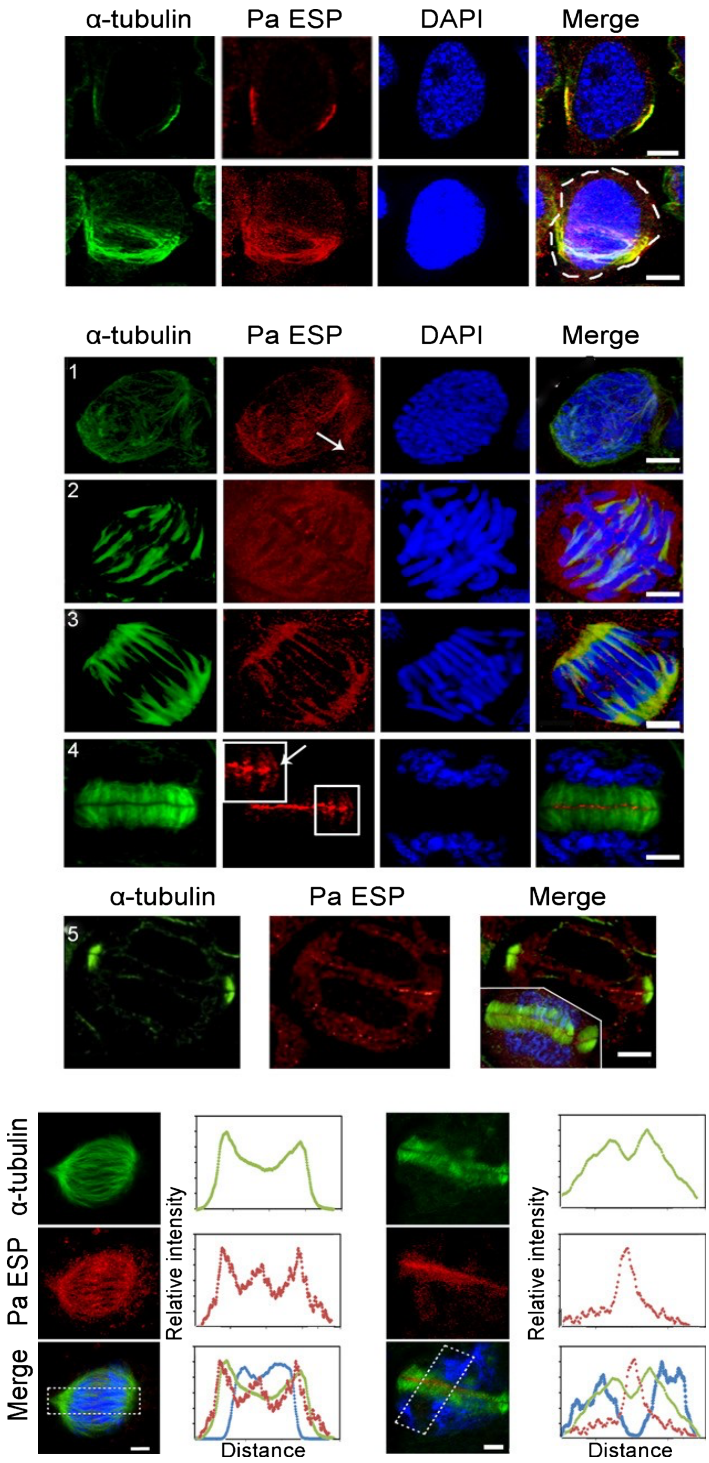

Fig. 3 Intracellular localization of Picea abies EXTRA SPINDLE POLES (Pa ESP). (a, b) Staining of Pa ESP (red), tubulin (green) and DNA (blue; 40,6-diamidino-2-phenylindole, DAPI) in the embryonic Norway spruce cells fixed with formaldehyde during (a) early prophase, (b1) prophase, (b2) metaphase, (b3) anaphase, (b4) telophase and (b5) late cytokinesis. In (a) upper images are from a single Z-axis optical section and lower images are maximal projection. The cell boundaries are denoted by the dotted line (lower). In (b1) the arrow denotes the peripheral preprophase band. The inset in (b4) shows a higher magnification of the phragmoplast leading edge. The arrow denotes association of Pa ESP with microtubules. The inset in (b5) shows the maximum projection image with DNA staining. Bars, 5 lm. (c, d) Staining of Pa ESP, tubulin and DNA in the embryonic cells fixed with methanol during anaphase (c) and telophase (d). Densitometry scans were performed in the framed areas. Different colours indicate Pa ESP (red), tubulin (green) and DNA (blue) intensities. Bars, 5 lm.

Pa ESP deficiency impairs early embryo development

To investigate the role of Pa ESP in embryogenesis we produced transgenic lines constitutively expressing a hairpin construct against Pa ESP (Pa ESP-RNAi; Figs 4, S1b). We could only obtain two viable cell lines (4.1 and 4.2), while the rest of the transgenic lines ceased proliferation following initial selection. Both lines exhibited significantly lower levels of Pa ESP (Figs 4a, S1b). Knockdown of Pa ESP inhibited the development of early embryos from PEMs upon withdrawal of PGR (Fig. 4b). WT cul-tures contained embryos with compact embryonal masses and sev-eral files of anisotropically expanding suspensor cells. By contrast, Pa ESP-RNAi lines contained irregularly formed embryonal masses connected to a suspensor-like structure composed of super-numerary cells showing impaired anisotropic expansion (Figs 4c, S3a,b). These cells were not part of the embyonal masses, which could be easily distinguished by bright fluorescein diacetate stain-ing (Fig. S4a; Methods S2). This implies that Pa ESP deficiency does not affect specification of the tube or suspensor cells, but rather inhibits their elongation (Fig. S3a). Consistently, these cells did not show high mRNA levels of the cell division-related genes Pa CYCBL1 (CyclinB-Like 1) and Pa RBRL (Retinoblastoma Like; Fig. S4b,c; Zhu et al., 2014). We noticed that some suspensor-like cells at the basal pole of the RNAi embryos showed apparent signs of cell death (staining with Evans blue; Fig. S5). However, these cells lacked any signs of proper anisotropic expansion.

To exclude the possibility that observed phenotype was a con-sequence of pleiotropic effects of the constitutive depletion of Pa ESP, we generated estradiol-inducible Pa ESP RNAi lines (Pa ESP-XVE > RNAi; Fig. S1a). Depletion of Pa ESP induced by estradiol (induction was done from early embryogenesis onwards) resulted in similar developmental defects as described for consti-tutive RNAi lines (Fig. S3a–c). No alteration in embryo mor-phology was observed in the noninduced Pa ESP-XVE > RNAi (data not shown).

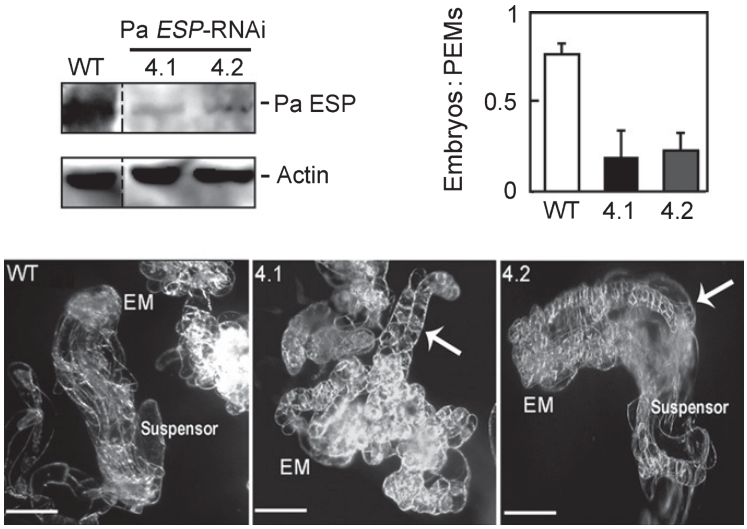

Fig. 4 Effect of Picea abies EXTRA SPINDLE POLES (Pa ESP) knockdown on early embryogenesis. (a) Western blot analysis of Pa ESP in wild-type (WT) and Pa ESP-RNAi cell lines of Norway spruce. The equal loading was confirmed using anti-actin. (b) Ratio of early embryos to proembryogenic masses (PEMs) in WT and Pa ESP-RNAi lines grown for 7 d without plant growth regulators (PGR). The data show means +_ SD of triplicate experiments. *, P < 0.01 (vs WT, Student's t-test). (c) Representative dark field microscopy images of early embryos from WT and Pa ESP-RNAi lines grown for 7 d without PGR. Arrows indicate formation of ectopic files of small cells instead of elongated suspensor cells. EM, embryonal mass. Bars, 100 lm.

Pa ESP is required for chromosome disjunction

To investigate the role of Pa ESP in sister chromatid separation, we stained Pa ESP-RNAi or Pa ESP-XVE > RNAi cells with DAPI (Fig. 5a). We failed to identify discernible chromosomal aberrations, suggesting that during the selection process we most likely counter-selected for lines that had sufficient levels of Pa ESP to sustain cell division. In fact, neither constitutive nor inducible expression of the Pa ESP-RNAi construct led to the reduction of the Pa ESP mRNA level to < 50% of control values (WT or noninduced, respectively) (Fig. S1).

We have overcome this limitation by the transient expression of the Pa ESP-RNAi construct mediated by A. tumefaciens (as detailed in the Materials and Methods section). We used a control vector expressing mRFP to estimate the percentage of cells transformed following A. tumefaciens transfection. Approximately 80% of cells showed detectable mRFP fluorescence under a con-focal microscope. Transient depletion of Pa ESP resulted in over 90% reduction of Pa ESP levels, when compared with mRFP transfected cells (determined by qRT-PCR; see also the Materials and Methods section). We assume that some cells should have even higher suppression of Pa ESP, considering that c. 20% of cells remained untransformed. Analysis of the transformed cells revealed a chromosome nondisjunction phenotype (Fig. 5a; 12 of 56 cells examined vs none of 67 in mRFP control) resembling the Arabidopsis rsw4 allele (Moschou et al., 2013). Complemen-tation experiments of the Arabidopsis rsw4 phenotype with Pa ESP showed that Pa ESP could rescue the chromatid nondisjunc-tion phenotype of rsw4 (Liu & Makaroff, 2006; Fig. 5b), but failed to rescue the root-swelling phenotype (Fig. S6). On the other hand, a point mutant of Pa ESP with a catalytic cysteine-to-glycine (C2147G) mutation failed to rescue chromatid nondis-junction (data not shown). Thus, Pa ESP performs the canonical role of ESP proteins in anaphase progression.

(a)

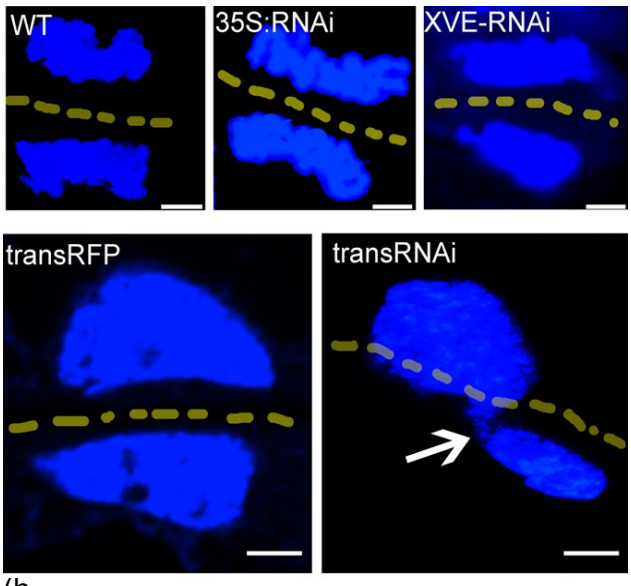

(b

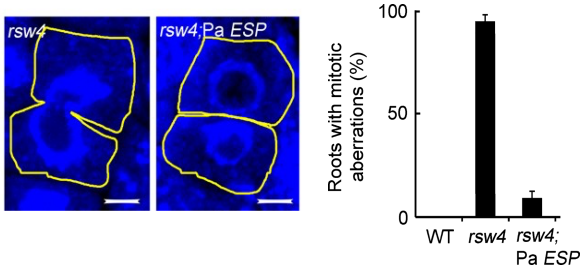

Fig. 5 Chromosomal aberrations in cells with transiently diminished Picea abies EXTRA SPINDLE POLES (Pa ESP) and complementation of rsw4 chromatid nondisjunction phenotype. (a) For detection of chromosomal aberrations, cells of Norway spruce were fixed and stained with 40,6-diamidino-2-phenylindole (DAPI). Images are from a single representative experiment repeated twice. As a control in transient assays, lines transiently expressing monomeric red fluorescent protein (mRFP) under a 35S promoter were used. Aberrations were never observed in these transformants. The arrow indicates chromosomal aberration. Yellow dotted lines demark the cell wall between chromosomes of daughter cells. trans, transient. Bars, 5 lm. (b) Complementation of nondisjunction phenotype in Arabidopsis rsw4 line p1 expressing Pa ESP (left) and the frequencies of roots with chromosomal aberrations (right). In rsw4, chromatid nondisjunction results in chromosomal bridges and improper karyokinesis, leading to the formation of nuclei dissected by a cell wall (similarly to what was reported by Moschou et al., 2013). Note that under our experimental conditions we did not observe chromosomal aberrations in wild-type (WT) plants. Yellow lines demark the cell periphery. The data shown in the chart are means +_ SD of triplicate experiments with 10–12 roots each. Bars, 2.5 lm.

Pa ESP is essential for late embryogenesis

We next compared the later stages of embryogenesis in WT and Pa ESP-deficient lines (Figs 6, S7). Whereas normally the cotyledonary embryos could be detected following 2 wk after transfer to the maturation medium containing ABA, the cotyledonary embryos in Pa ESP-RNAi or Pa ESP-XVE > RNAi lines formed only after 10 wk (Figs 6a, S7a,b). Notably, the cotyledonary embryos eventually formed in the RNAi lines, but exhibited a

range of morphological abnormalities, including misshapen and missing cotyledons, short hypocotyls, and split embryos (Fig. 6b, c). Histological examination revealed that cells in the hypocotyls of the cotyledonary embryos were enlarged and showed reduced anisotropy (Figs 6d,e, S8).

In order to examine whether these phenotypes are associated with chromatid nondisjunction or other mitotic aberrations, we performed microscopic examination of the DNA after staining with DAPI. We checked sections of the WT and mutant lines and examined 1848 DAPI-stained nuclei (of these, 653 in WT, 595 in Pa ESP-RNAi and 600 in Pa ESP-XVE > RNAi). None of these nuclei revealed discernible nondisjunction phenotype. From these cells, only 20 cells (c. 0.1%) were at the metaphase stage (nine in WT, six in Pa ESP-RNAi, and four in the Pa ESP-XVE > RNAi). Such a limited dataset precludes us from drawing conclusions regarding mitotic aberrations other than chromatid nondisjunction.

To overcome this limitation, we examined the shoot apical meristem region of cotyledonary embryos where c.2% of WT cells showed mitotic features (51 out of 2550 cells). In Pa ESP-RNAi and in Pa ESP-XVE > RNAi, only 0.5% of the cells had mitotic features (17 out of 3528 cells for Pa ESP-RNAi; 21 out of 3540 cells for Pa ESP-XVE > RNAi). However, no discernible mitotic abnormalities were observed. In the WT we identified 14 cells (out of 51), while in Pa ESP-RNAi we identified three and in Pa ESP-XVE > RNAi we identified four (out of 27 and 21 cells, respectively) that were in anaphase. Taken together, these observations suggest that mitotic cells are less frequent in the mutant lines and their developmental defects are not caused by chromosomal aberrations.

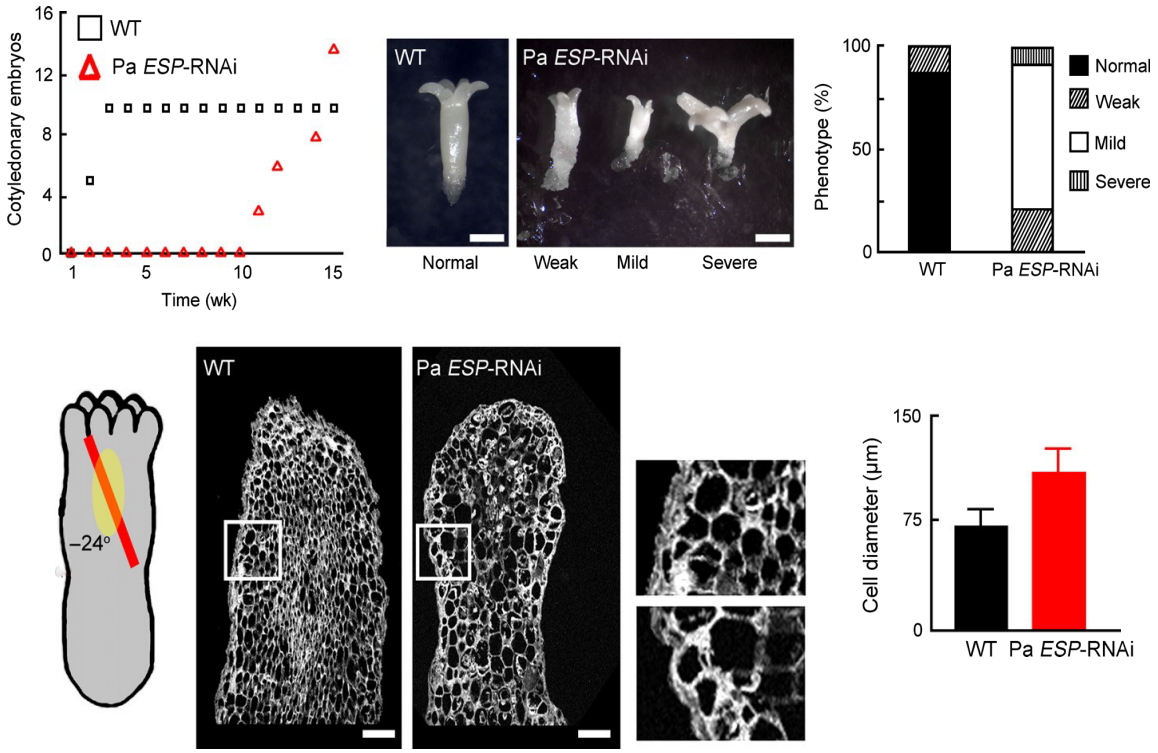

Fig. 6 Effect of Picea abies EXTRA SPINDLE POLES (Pa ESP) knockdown on the development of cotyledonary embryos. (a) Time course analysis of Norway spruce cotyledonary embryo formation in wild-type (WT) and Pa ESP-RNAi line 4.1. Numbers on the y-axis are absolute numbers (embryos formed). Data are from a single representative experiment, which was repeated three times with similar results. (b) Classes of cotyledonary embryo phenotypes observed in the WT and Pa ESP-RNAi line 4.1. Normal, cotelydonary embryos showing radial symmetry and average size; weak, cotelydonary embryos with disturbed radial symmetry and decreased size; severe, cotelydonary embryos showing scission and/or loss of radial symmetry and/or size aberrations; mild, in between the weak and severe classes. Bars, 5 mm. (c) Frequency distribution of distinct phenotypes of cotyledonary embryos in WT and Pa ESP-RNAi line 4.1. Note the absence of normal embryos in the RNAi line. Data are from a single representative experiment, which was repeated three times with similar results. (d) Sections of hypocotyls from cotyledonary embryos of WT and Pa ESP-RNAi line 4.1 (severe class). The red line on the cartoon illustrates orientation of the section, and the faint yellow ellipse indicates the region of the shoot apical meristem. Shown on the right are the enlarged boxed areas. Bars, 300 lm. (e) Diameter of hypocotyl cells of cotyledonary embryos from WT and Pa ESP-RNAi lines. The data show means +_ SD of triplicate experiments, each containing at least 10 tissue sections. *, $P < 0.01$ (vs WT, Student's t-test).

Pa ESP deficiency affects microtubule stability

As polarized development depends on cell expansion, which is in turn controlled by microtubules, we examined microtubule orga-nization in early and cotyledonary embryos. The microtubules in elongating suspensor cells evaded analyses owing to their highly fragmented nature (see also Smertenko et al., 2003). Knockdown of Pa ESP caused no significant alterations in the random organi-zation of cortical microtubules in the embryonal mass cells (Fig. 7a; Smertenko et al., 2003). By contrast, cortical micro-tubule bundles in the tube cells of Pa ESP-RNAi showed reduced density (Fig. 7a,b). Similarly, the density of cortical microtubule bundles in the hypocotyl cells of Pa ESP-RNAi cotyledonary embryos was reduced (Fig. 7a,b). Furthermore, while the major-ity (c. 70%) of microtubules in the hypocotyl cells of cotyle-donary WT embryos were transverse, in the Pa ESP-RNAi lines they were predominantly oblique or longitudinal (Fig. 7c). Taken together, these results demonstrate that despite a significant reduction of Pa ESP expression during cell differentiation, its activity remains critical for regulation of both microtubule orga-nization and cell elongation.

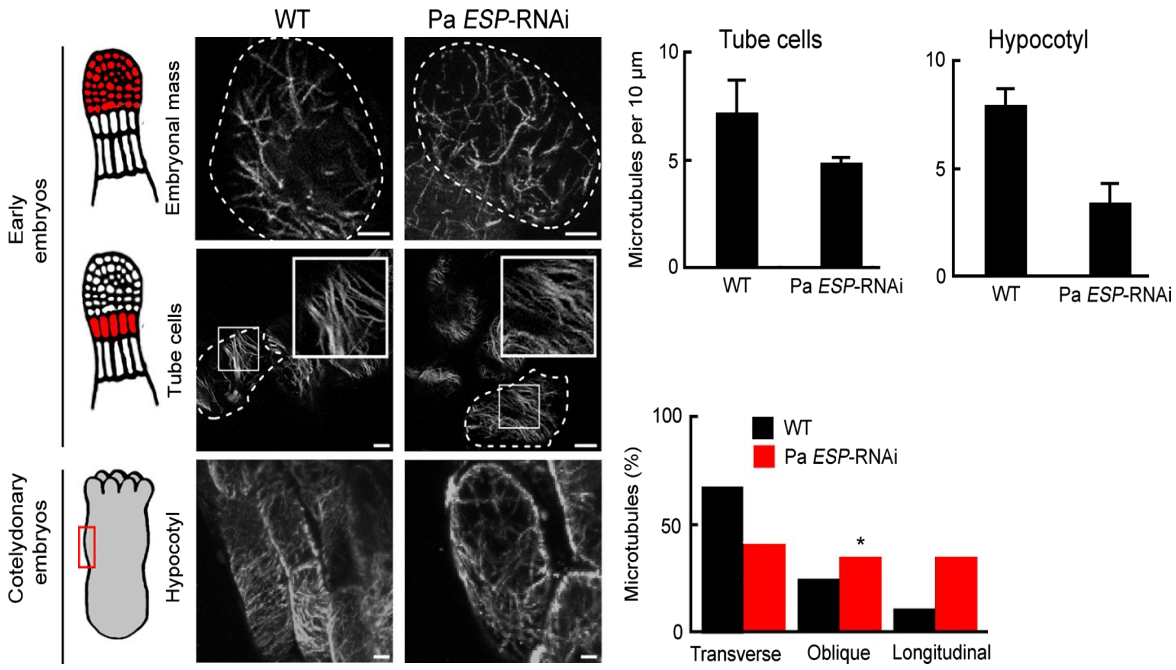

Fig. 7 Effect of Picea abies EXTRA SPINDLE POLES (Pa ESP) knockdown on the organization of cortical microtubules. (a) Cortical microtubules in embryonal mass and tube cells of early embryos and hypocotyl cells of cotyledonary embryos from wild-type (WT) and Pa ESP-RNAi line 4.1 of Norway spruce. Insets show higher magnification of boxed areas. Bars, 10 lm. (b) Microtubule density (number of microtubules per 10 lm) in the embryonal tube cells and hypocotyl cells from WT and Pa ESP-RNAi line 4.1. The data show means □ SD of triplicate experiments, each including 60 cells analysed.*, $P < 0.05$ (vs WT, two-sided Dunnett's test). (c) Orientation of microtubules (percentage of microtubules in each particular orientation) in the hypocotyl cells from WT and Pa ESP-RNAi line 4.1. Data are from a single representative experiment, which was repeated twice, each time including 60 cells.*, $P < 0.05$ (vs WT, Fisher's exact test).

Discussion

Diversification of ESP proteins

All ESP proteins identified so far share a caspase-haemoglobinase fold characteristic for the CD clan of cysteine proteases, which includes clostripains, legumains, gingipains, caspases, paracas-pases and metacaspases (Aravind & Koonin, 2002). Apart from this conserved fold, the primary structure of ESP lacks a signifi-cant conservation (Notes S1). For example, Pa ESP is devoid of the Ca2+-binding EF-hand and 2Fe-2S motifs found in At ESP. However, whether these motifs serve any function remains unclear.

Phylogenetic analysis reveals that ESP homologues of green, brown, diatom algae and land plants form independent clades (Fig. 1a). This pattern suggests that besides the role in daugh-ter chromatid disjunction, ESP evolved specific functions in each lineage. The monophyletic nature of the land plant clade indicates that structure and functions of ESP coevolved with increased complexity of plant morphology and life cycle. The primary structure of ESP in Streptophyta appears to have undergone significant alterations with development of the multicellular body plan in Klebsormidium, and then with evo-lution of the phragmoplast and

colonization of land in Embryophytes (Leliaert et al., 2011). Another round of sub-stantial modifications of the ESP structure has happened with the evolution of angiosperms.

Role of Pa ESP in cell division and microtubule organization

Extra Spindle Poles from different lineages reveal variable intra-cellular localization pattern. Yeast ESP associates with spindle poles and microtubules of anaphase spindle, whereas human ESP was found only on the metaphase spindle poles and then became cytoplasmic in anaphase (Jensen et al., 2001; Chestukhin et al., 2003). Arabidopsis ESP associates with microtubules of the prophase, metaphase and anaphase spindle, as well as phragmo-plast microtubules and cell plate (Moschou et al., 2013).

Similar to At ESP, Pa ESP associates with microtubules during the interphase, prophase, metaphase and anaphase, and then associates with the phragmoplast microtubules, midzone and cell plate during telophase. Pa ESP remains associated with the cell plate after disassembly of the phragmoplast microtubules, sug-gesting that it might be required for vesicle trafficking to the maturing cell plate. Consistent with this conclusion, At ESP was found to temporally colocalize with RabA2a-specific endosomes (Moschou et al., 2013).

In our experiments, constitutive down-regulation of Pa ESP did not result in chromosome nondisjunction and cytokinetic defects observed in other species, including Arabidopsis (Fig. 5; Liu & Makaroff, 2006; Wu et al., 2010; Moschou et al., 2013). Furthermore, despite association of Pa ESP with mitotic micro-tubule arrays, no discernible abnormalities in their organization were observed in the Pa ESP-RNAi lines. The most likely expla-nation for normal cell divisions in the Pa ESP-RNAi lines is the incomplete gene silencing still allowing production of a sufficient amount of protein (Fig. 4a) that sustains anaphase transition. Accordingly, a more efficient reduction of Pa ESP using the tran-sient transformation method that we established here revealed the requirement of Pa ESP for chromosome disjunction. Therefore, Pa ESP plays a canonical role in the metaphase–anaphase transi-tion. Although in constitutive RNAi lines the abundance of Pa ESP was sufficient to ensure a normal anaphase progression, the reduced number of meristematic cells in the hypocotyls of Pa ESP-deficient embryos may suggest that Pa ESP is required for the regulation of meristem size, independently of its role in anaphase. Alternatively, the reduced meristem size could be a pleiotropic effect of the retarded embryo development in the Pa ESP-deficient lines.

Consistent with the specific functions of ESP in different lin-eages, Pa ESP failed to rescue the root-swelling phenotype of Arabidopsis rsw4, although previously this phenotype could be complemented by At ESP (Fig. 5b; Moschou et al., 2013). Con-sidering that Pa ESP could complement the chromatid nondis-junction phenotype of rsw4 and its knockdown in P. abies results in chromatid nondisjunction, Pa ESP appears to be a functional homologue of canonical ESP proteins. These findings suggest dif-ferent effector mechanisms underlying the functions of ESP in anaphase progression and in controlling anisotropic cell expan-sion.

In contrast to the unaltered microtubule arrays in the embry-onal masses, the cortical microtubules in tube cells, and especially in epidermis and cortex cells of cotyledonary embryos of Pa ESP-RNAi lines, exhibited reduced density and length, as well as altered orientation (Fig. 7). The hypocotyl cells in the Pa ESP-deficient embryos were bigger than in the WT, indicating that abnormal microtubule organization was associated with irregular cell expansion (Baskin, 2001; Wasteneys, 2004; Baskin & Gu, 2012). This implies that regulation of microtubule dynamics in cells engaged in anisotropic growth are more sensitive to the loss

of Pa ESP function than proliferating cells of early embryos, which can tolerate a reduced abundance of Pa ESP protein. Therefore, Pa ESP could facilitate stabilization of microtubules which define the elongation axis. Pa ESP may not function directly in microtubule regulation, but instead may regulate cell wall functions that affect microtubule orientation and dynamics. We assume that Pa ESP function in the regulation of micro-tubules or cell wall could be noncell-autonomous, involving mobile signals produced in meristematic cells. Furthermore, we cannot exclude the possibility that morphological defects observed in Pa ESP-RNAi lines directly impact the flux of mobile signals such as auxin. This function of Pa ESP is consistent with our findings that elongating cells with undetectable Pa ESP (e.g. tube cells) are affected when Pa ESP is depleted in proximal meristematic cells (e.g. embryonal mass cells).

Pa ESP is required for elongation of the suspensor

Norway spruce embryos at the early embryogeny stage undergo polarization and forms two domains with distinct developmental fates: proliferating embryonal mass and terminally differentiated suspensor, including the uppermost layer of tube cells (Fig. 2a; Bozhkov et al., 2005). Pa ESP protein could be detected using antibody only in the embryonal masses, while the degree of pro-tein accumulation in the elongating embryo-suspensors, tube cells and seedlings was below detection limits. In accordance with the western blotting data, qRT-PCR demonstrated significant down-regulation of ESP in all organs or tissues but embryonal mass.

Our reverse genetics experiments suggest that Pa ESP is criti-cally required to sustain cell elongation during embryogeny. Developmental defects induced by Pa ESP deficiency resemble the phenotype of spruce embryos grown in the presence of polar auxin transport inhibitor, 1-N-naphtylphthalamic acid (Larsson et al., 2008). For example, in both cases, the fate of suspensor cells was affected and supernumerary suspensor-like cells could be detected instead of normally elongating cells. It is plausible that, as in Arabidopsis root cells (Moschou et al., 2013), inhibi-tion of Pa ESP perturbs auxin signalling and in this way interferes with the cell expansion.

Conclusion

Here, we were able to dissect two functions of ESP by showing that a gymnosperm homologue could complement the chromo-some nondisjunction phenotype of rsw4, but not the root-swelling phenotype. This cell division-unrelated function of ESP could be attributed to the regulation of polarized vesicular trafficking. So far, no robust molecular markers of cell polarity have been estab-lished for gymnosperms. However, recent advances in gym-nosperm genomics and an increasing number of fully sequenced gymnosperm genomes should help to overcome these limitations (Birol et al., 2013; Nystedt et al., 2013; Zimin et al., 2014).

Acknowledgements

The authors are grateful to Tsuyoshi Nakagawa for sharing pub-lished research materials and Alison Ritchie for the assistance in preparation of anti-Pa ESP. This work was supported by grants from the VR Swedish Research Council (to P.N.M. and P.V.B.), Pehrssons Fund (to P.V.B.), the Swedish Foundation for Strate-gic Research (to P.V.B.), the Olle Engkvist Foundation (to P.V.B.), the Knut and Alice Wallenberg Foundation (to P.V.B.), the August T. Larsson Foundation (to A.P.S. and P.V.B.), Hatch Grant WNP00826 (to A.P.S.), and a Spanish Ministry of Science and Innovation grant (AGL2010-15684 to M.F.S). V.S-V. was recipient of a FPI fellowship from the Spanish Ministry of Science and Innovation (BES-2008-003592).

Author contributions

P.N.M., E.I.S., E.A.M., K.F., S.H.R., E.G.-B., A.P.S. and V.S-V., performed the research; P.N.M., A.P.S., P.V.B., designed the research; P.N.M., A.P.S., P.V.B. wrote the article; M.F.S. and P.J.H. offered materials/analytical methods. All authors approved the final version of the manuscript.

References

Aravind L, Koonin EV. 2002. Classification of the caspase-hemoglobinase fold: detection of new families and implications for the origin of the eukaryotic separins. Proteins 46: 355–367.

von Arnold S, Sabala I, Bozhkov P, Dyachok J, Filonova L. 2002.Developmental pathways of somatic embryogenesis. Plant Cell Tissue andOrgan Culture 69: 233–249.

Baskin TI. 2001. On the alignment of cellulose microfibrils by corticalmicrotubules: a review and a model. Protoplasma 215: 150–171.

Baskin TI, Gu Y. 2012. Making parallel lines meet: transferring informationfrom microtubules to extracellular matrix. Cell Adhesion and Migration 6: 404–408.

Bembenek JN, White JG, Zheng YX. 2010. A role for separase in the regulationof RAB-11-positive vesicles at the cleavage furrow and midbody. CurrentBiology 20: 259–264.

Birol I, Raymond A, Jackman SD, Pleasance S, Coope R, Taylor GA, SaintYuen MM, Keeling CI, Brand D, Vandervalk BP et al. 2013. Assembling the20 Gb white spruce (Picea glauca) genome from whole-genome shotgunsequencing data. Bioinformatics 29: 1492–1497.

Bozhkov PV, Filonova LH, Suarez MF. 2005. Programmed cell death in plantembryogenesis. Current Topics in Developmental Biology 67: 135–179.

Brand L, Horler M, Nuesch E, Vassalli S, Barrell P, Yang W, Jefferson RA,Grossniklaus U, Curtis MD. 2006. A versatile and reliable two-componentsystem for tissue-specific gene induction in Arabidopsis. Plant Physiology 141:1194–1204.

Capron A, Chatfield S, Provart N, Berleth T. 2009. Embryogenesis: patternformation from a single cell. Arabidopsis Book 7: e0126.

Chestukhin A, Pfeffer C, Milligan S, DeCaprio JA, Pellman D. 2003.Processing, localization, and requirement of human separase for normalanaphase progression. Proceedings of the National Academy of Sciences, USA 100:4574–4579.

Ciosk R, Zachariae W, Michaelis C, Shevchenko A, Mann M, Nasmyth K.1998. An ESP1/PDS1 complex regulates loss of sister chromatid cohesion atthe metaphase to anaphase transition in yeast. Cell 93: 1067–1076.

Filonova LH, Bozhkov PV, Brukhin VB, Daniel G, Zhivotovsky B, von ArnoldS. 2000. Two waves of programmed cell death occur during formation anddevelopment of somatic embryos in the gymnosperm, Norway spruce. Journal of Cell Science 24: 4399–4411.

Filonova LH, Suarez MF, Bozhkov PV. 2008. Detection of programmed celldeath in plant embryos. Methods in Molecular Biology 427: 173–179.

van der Hoorn RAL. 2008. Plant proteases: from phenotypes to molecularmechanisms. Annual Review of Plant Biology 59: 191–223.

Jensen S, Segal M, Clarke DJ, Reed SI. 2001. A novel role of the buddingyeast separin Esp1 in anaphase spindle elongation: evidence that proper spindle association of Esp1 is regulated by Pds1. Journal of Cell Biology 152:27–40.

Johnson KL, Degnan KA, Walker JR, Ingram GC. 2005. AtDEK1 is essential forspecification of embryonic epidermal cell fate. Plant Journal 44: 114–127.

Kanei M, Horiguchi G, Tsukaya H. 2012. Stable establishment of cotyledonidentity during embryogenesis in Arabidopsis by ANGUSTIFOLIA3 andHANABA TARANU. Development 139: 2436–2446.

Laemmli UK. 1970. Cleavage of structural proteins during the assembly of thehead of bacteriophage T4. Nature 227: 680–685.

Larsson E, Sitbon F, Ljung K, von Arnold S. 2008. Inhibited polar auxintransport results in aberrant embryo development in Norway spruce. NewPhytologist 177: 356–366.

Leliaert F, Verbruggen H, Zechman FW. 2011. Into the deep: new discoveries atthe base of the green plant phylogeny. BioEssays 33: 683–692.

Lid SE, Olsen L, Nestestog R, Aukerman M, Brown RC, Lemmon B, Mucha M,Opsahl-Sorteberg HG, Olsen OA. 2005. Mutation in the Arabidopisis thalianaDEK1 calpain gene perturbs endosperm and embryo development while overexpressionaffects organ development globally. Planta 221: 339–351.

Liu Z, Makaroff CA. 2006. Arabidopsis separase AESP is essential for embryodevelopment and the release of cohesin during meiosis. Plant Cell 18: 1213–1225.

Mayer U, Ruiz RAT, Berleth T, Misera S, Jurgens G. 1991. Mutations affectingbody organization in the Arabidopsis embryo. Nature 353: 402–407.

Meinke DW. 1991. Perspectives on genetic-analysis of plant embryogenesis.Plant Cell 3: 857–866.

Minina EA, Filonova LH, Fukada K, Savenkov EI, Gogvadze V, Clapham D,Sanchez-Vera V, Suarez MF, Zhivotovsky B, Daniel G et al. 2013. Autophagy and metacaspase determine the mode of cell death in plants. Journal of CellBiology 203: 917–927.

Moschou PN, Bozhkov PV. 2012. Separases: biochemistry and function.Physiologia Plantarum 145: 67–76.

Moschou PN, Smertenko AP, Minina EA, Fukada K, Savenkov EI, Robert S,Hussey PJ, Bozhkov PV. 2013. The caspase-related protease separase (EXTRASPINDLE POLES) regulates cell polarity and cytokinesis in Arabidopsis. PlantCell 25: 2171–2186.

Nakagawa T, Kurose T, Hino T, Tanaka K, Kawamukai M, Niwa Y, ToyookaK, Matsuoka K, Jinbo T, Kimura T. 2007. Development of series of gatewaybinary vectors, pGWBs, for realizing efficient construction of fusion genes forplant transformation. Journal of Biosciences and Bioengineering 104: 34–41.

Nystedt B, Street NR, Wetterbom A, Zuccolo A, Lin YC, Scofield DG, Vezzi F,Delhomme N, Giacomello S, Alexeyenko A et al. 2013. The Norway sprucegenome sequence and conifer genome evolution. Nature 497: 579–584.

Pennell RI, Janniche L, Scofield GN, Booij H, Devries SC, Roberts K. 1992.Identification of a transitional cell state in the developmental pathway to carrotsomatic embryogenesis. Journal of Cell Biology 119: 1371–1380.

Saitou N, Nei M. 1987. The neighbor-joining method – a new method forreconstructing phylogenetic trees. Molecular Biology and Evolution 4: 406–425.

Singh HE. 1978. Embryology of gymnosperms. Handbuch der Pflanzenanatomie.Berlin, Germany: Gebruder Borntraeger.Smertenko A, Bozhkov PV. 2014. Somatic embryogenesis: life and deathprocesses during apical–basal patterning. Journal of Experimental Botany 65:1343–1360.

Smertenko AP, Bozhkov PV, Filonova LH, von Arnold S, Hussey PJ. 2003. Reorganisationof the cytoskeleton during developmental programmed cell deathin Picea abies embryos. Plant Journal 33: 813–824.

Smertenko AP, Hussey PJ. 2008. Immunolocalization of proteins in somaticembryos – applications for studies on the cytoskeleton. Methods in MolecularBiology 427: 157–171.

Suarez MF, Filonova LH, Smertenko A, Savenkov EI, Clapham DH, vonArnold S, Zhivotovsky B, Bozhkov PV. 2004. Metacaspase-dependent programmed cell death is essential for plant embryogenesis. Current Biology 14:R339–R340.

Sun YX, Kucej M, Fan HY, Yu H, Sun QY, Zou H. 2009. Separase is recruitedto mitotic chromosomes to dissolve sister chromatid cohesion in a DNAdependentmanner. Cell 137: 123–132.

Tanaka H, Onouchi H, Kondo M, Hara-Nishimura I, Nishimura M, MachidaC, Machida Y. 2001. A subtilisin-like serine protease is required for epidermal surface formation in Arabidopsis embryos and juvenile plants. Development 128:4681–4689.

Ueda M, Laux T. 2012. The origin of the plant body axis. Current Opinion inPlant Biology 15: 578–584.Wasteneys GO. 2004. Progress in understanding the role of microtubules inplant cells. Current Opinion in Plant Biology 7: 651–660.

Wendrich JR, Weijers D. 2013. The Arabidopsis embryo as a miniaturemorphogenesis model. New Phytologist 199: 14–25.

Wu S, Scheible WR, Schindelasch D, Van Den Daele H, De Veylder L, BaskinTI. 2010. A conditional mutation in Arabidopsis thaliana separase induceschromosome non-disjunction, aberrant morphogenesis and cyclin B1;1stability. Development 137: 953–961.

Yang XH, Boateng KA, Yuan L, Wu S, Baskin TI, Makaroff CA. 2011. TheRadially Swollen 4 separase mutation of Arabidopsis thaliana blockschromosome disjunction and disrupts the radial microtubule system inmeiocytes. PLoS One 6: e19459.

Zhu T, Moschou PN, Alvarez JM, Sohlberg JJ, von Arnold S. 2014. Wuschelrelatedhomeobox 8/9 is important for proper embryo patterning in thegymnosperm Norway spruce. Journal of Experimental Botany 65: 6543–6552.

Zimin A, Stevens KA, Crepeau M, Holtz-Morris A, Koriabine M, Marcais G,Puiu D, Roberts M, Wegrzyn JL, de Jong PJ et al. 2014. Sequencing andassembly of the 22-Gb loblolly pine genome. Genetics 196: 875–890.Supporting Information

Additional Supporting Information may be found online in the Supporting Information tab for this article:

Fig. S1 Relative expression levels of Pa ESP in WT, Pa ESP RNAi

or Pa ESP XVE> RNAi lines.

Fig. S2 Intracellular localization of Pa ESP in interphase embryonal

mass cells and differentiated tube cells.

Fig. S3 Width, length and number of tube and suspensor cells and

potency for embryo formation, as affected by Pa ESP deficiency.

Fig. S4 Staining of the embryonal mass with fluorescein diacetate

and suspensor cells with Evans blue and Sytox orange of Pa ESPRNAi

and relative expression levels of Pa CYCBL1 and Pa RBRL

in WT and Pa ESP-RNAi.

Fig. S5 Evans blue staining of suspensor cells in the WT and Pa

ESP-RNAi.

Fig. S6 Pa ESP does not complement the rsw4 root-swelling phenotype.

Fig. S7 Effect of inducible Pa ESP knockdown on the morphology

of cotyledonary embryos.

Fig. S8 Width and length of embryos hypocotyl cells, as affected by Pa ESP deficiency.

Table S1 List of primers

Methods S1 Western blot analysis of Pa ESP protein.

Methods S2 Fluorescein diacetate staining of embryonal mass.

Notes S1 Alignment of ESP proteins.

Notes S2 Accession numbers.

***New Phytologist* Supporting Information**

Article title: ***EXTRA SPINDLE POLES* (Separase) controls anisotropic cell expansion in Norway spruce (*Picea abies*) embryos independently from its role in anaphase progression**

Authors: Panagiotis N. Moschou, Eugene I. Savenkov*, Elena A. Minina*, Kazutake Fukada*, Salim Hossain Reza, Emilio Gutierrez-Beltran, Victoria Sanchez-Vera, Maria F. Suarez, Patrick J. Hussey, Andrei P. Smertenko and Peter V. Bozhkov

Article acceptance date: 07 April 2016

The following Supporting Information is available for this article:

Fig. S1-8
Table S1
Method S1-2
Notes S2

Fig. S1. Relative expression levels of Pa *ESP* in WT, Pa *ESP*-RNAi or Pa *ESP*XVE> RNAi lines. (**a**) Comparison of relative Pa *ESP* mRNA levels in embryonal masses (EM), suspensors (S), cotyledons (C), hypocotyls (H) and roots (R) of WT line. Normalization was done against *PHOS*, *CDC2* and *EF1a*. The data show mean ± standard deviation of triplicate experiments with three technical replicates each. Different letters indicate significant differences at $P<0.05$ (n=3; Student's *t*-test). (**b**) Relative mRNA levels of Pa *ESP* in WT, Pa *ESP*-RNAi and Pa *ESP*-XVE>RNAi lines. Normalization was done against *CDC2* and *EF1a*. (-), absence and (+), presence of 20 μM estradiol. The data show mean ± standard deviation of triplicate experiments with three technical replicates each. *, $P<0.01$; *vs* WT, Student's *t*-test.

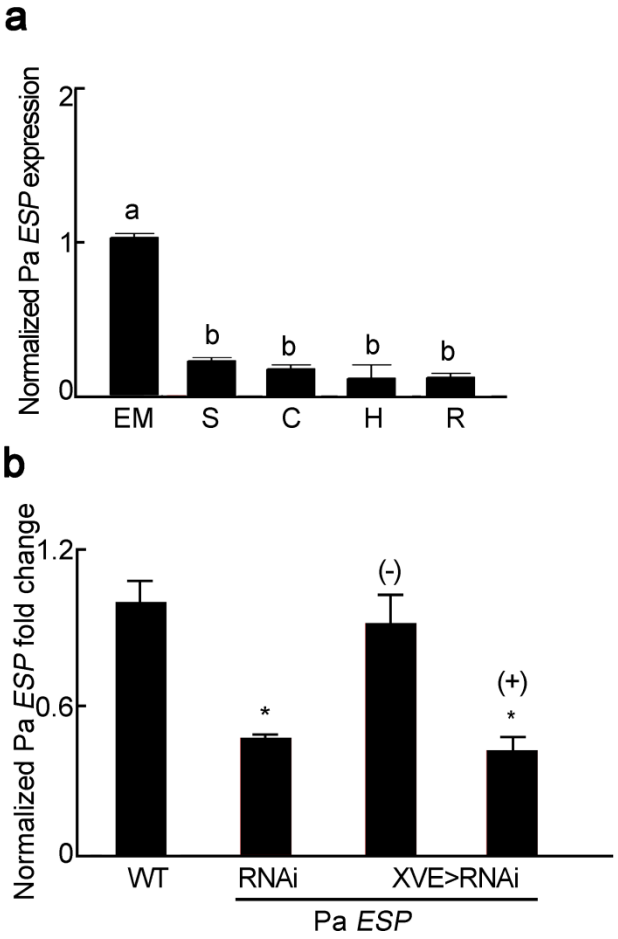

Figure S1

Fig. S2. Intracellular localization of Pa ESP in interphase embryonal mass cells and differentiated tube cells.
Staining of Pa ESP, tubulin, and DNA in the fixed embryonal mass cells during interphase (top images), and tube cells (bottom images). DNA staining with DAPI is not apparent in the tube cells in this focal plane. Note the absence of Pa ESP labelling in tube cells. Scale bars, 5 μm.

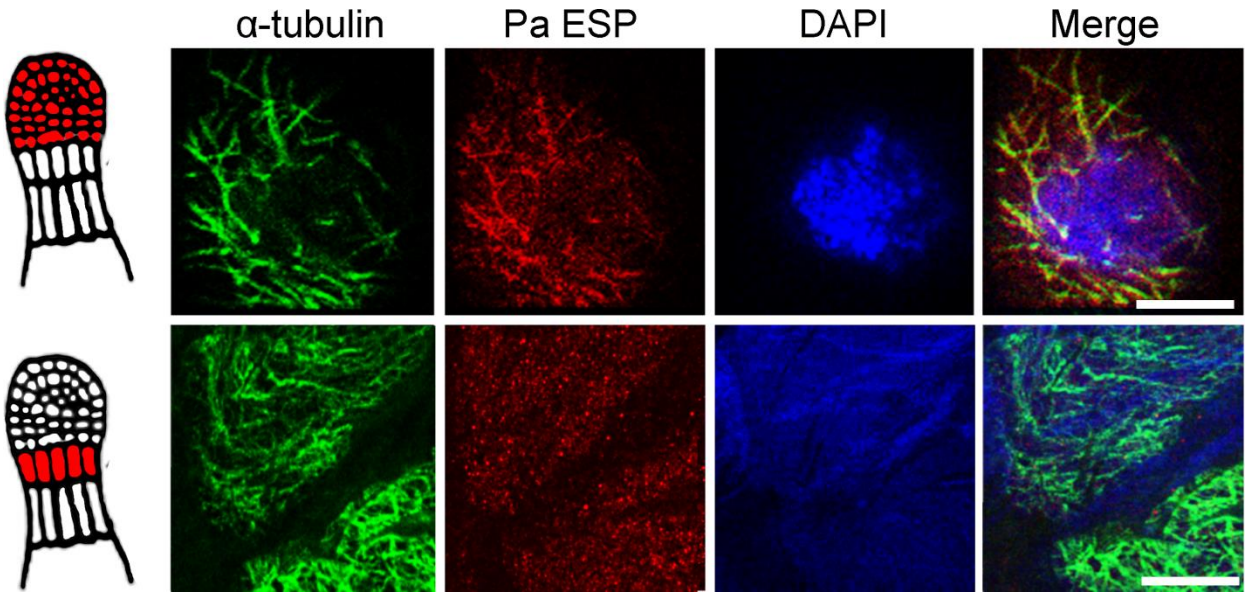

Figure S2

Fig. S3. Width, length and number of tube and suspensor cells and potency for embryo formation, as affected by Pa ESP deficiency.

(a) Length and width of tube cells in Pa *ESP* constitutive (RNAi) or inducible (XVE) lines. (**b**) Number of cells in a single individual cell file within suspensor domain was also estimated. Note that in these calculations, all cells situated below the embryonal mass were calculated, irrespective of their morphology. The ends of the box in (**a**) and (**b**) indicate the 25-75% quantiles and the vertical line within the box the median. Red whiskers extend from the ends of the box to the outermost data point that falls within the distances computed as follows '3rd quartile + 1.5×(interquartile range)' and '1st quartile - 1.5×(interquartile range)' where 'interquartile range' is the difference between the 1st and 3rd quartiles. If the data points do not reach the computed ranges, then the whiskers are determined by the upper and lower data point values (not including outliers). Blue whiskers indicate the 10% and 90% quartiles. Different values are indicated with black circles (n=20) and data are from a single representative experiment replicated three times. *P* values (comparison to WT) are indicated and were calculated using the non-parametric Wilcoxon test, since values were not normally distributed in the mutants. (**c**) Ratio of early embryos to PEMs in WT and Pa *ESP*-XVE>RNAi line 5.1 grown for seven days without PGR. The data show mean ± standard deviation of triplicate experiments with 30 embryos each. *, $P<0.01$; *vs* WT, Student's *t*-test.

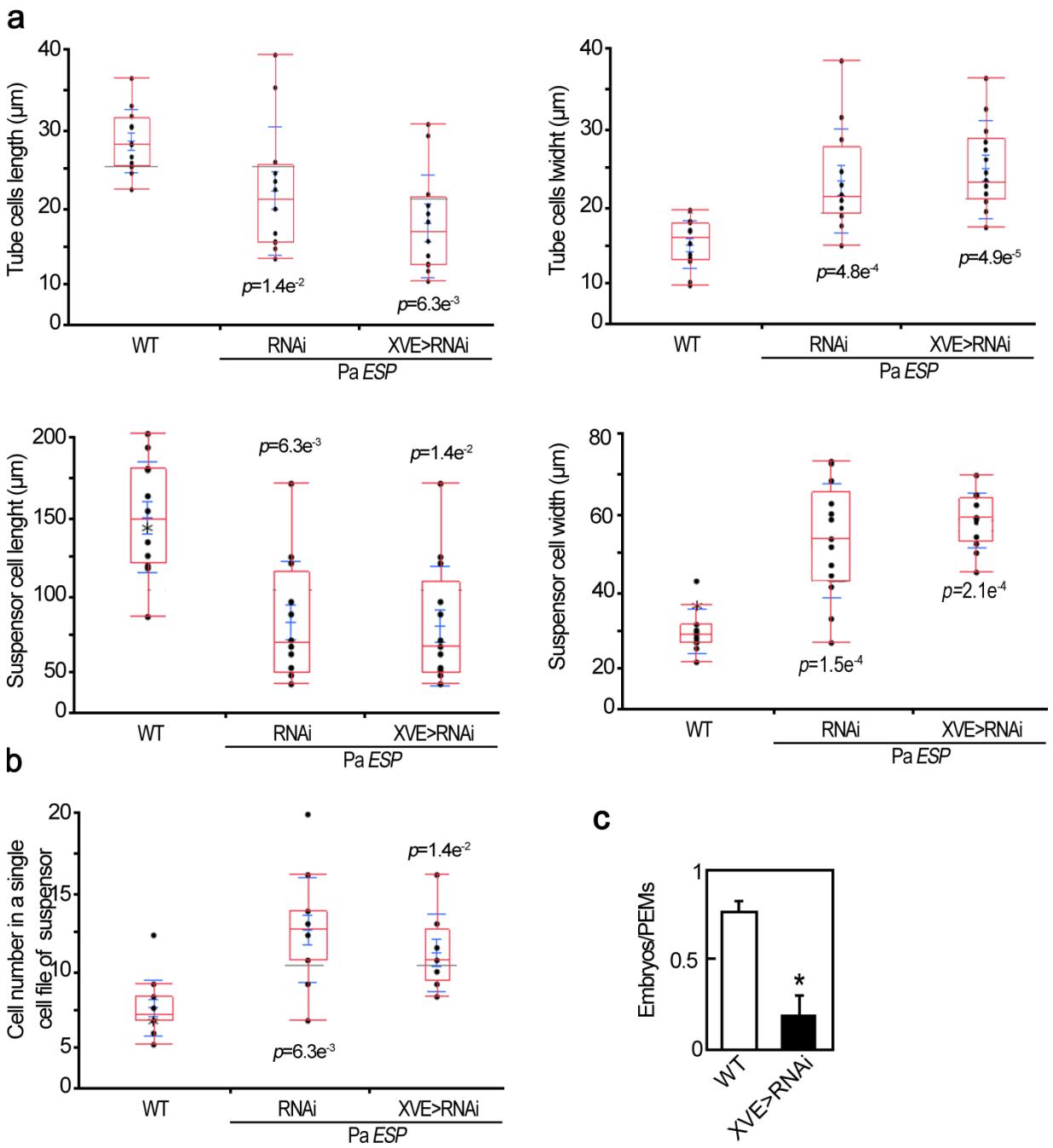
a
Tube cells length (µm)
40
30
20
10
0
p=1.4e-2
p=6.3e-3
WT
RNAi
XVE>RNAi
Pa ESP
Tube cells lwidht (µm)
p=4.8e-4
p=4.9e-5
Suspensor cell lenght (µm)
200
150
100
50
p=6.3e-3
p=1.4e-2
Suspensor cell width (µm)
80
60
40
20
p=1.5e-4
p=2.1e-4
b
Cell number in a single cell file of suspensor
15
10
5
c
Embryos/PEMs
1
0.5
*

Figure S3

Fig. S4. Staining of the embryonal mass with fluorescein diacetate and suspensor cells with Evan's blue and Sytox orange (see also Method S2) of Pa *ESP*-RNAi and relative expression levels of Pa *CYCBL1* and Pa *RBRL* in WT and Pa *ESP*-RNAi. (**a**) Staining of suspensor cells with Evan's blue (left). Embryonal mass (green) and suspensor cells (red nucleus) staining with fluorescein diacetate and Sytox Orange, respectively (right). Note the aberrant shape of the single suspensor cell in embryos grown in the presence of PGR. (**b**) Comparison of relative Pa *CYCBL1* mRNA levels in embryonal masses (EM) and suspensors (S) of WT line and Pa *ESP*-RNAi. (**c**) Comparison of relative Pa *RBRL* mRNA levels in embryonal masses (EM) and suspensors (S) of WT line and Pa *ESP*-RNAi. In (**b**) and (**c**) normalization was done against *PHOS*, *CDC2* and *EF1a*. The data show mean ± standard deviation of triplicate experiments with three technical replicates each. Different letters indicate significant differences at $P<0.05$ (n=3; Student's *t*-test).

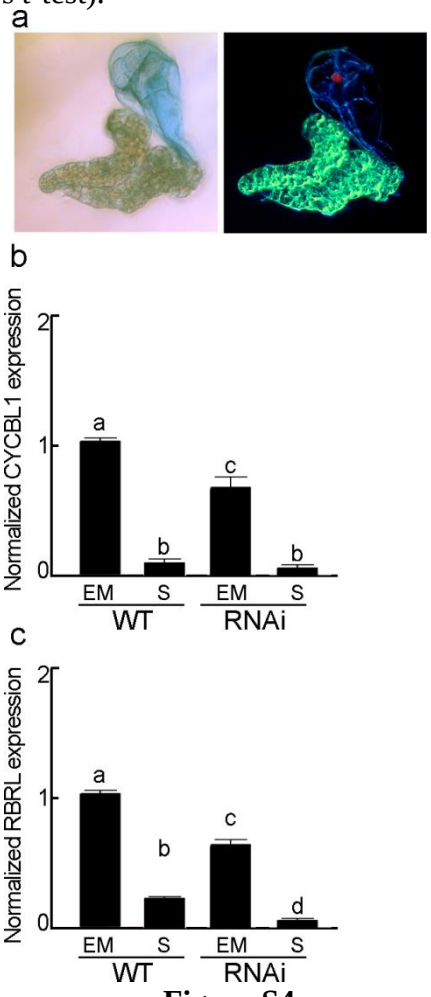

Figure S4

Fig. S5. Evan's blue staining of suspensor cells in WT and Pa ESP-RNAi.
(**a**) Note the formation of elongated Evan's blue positive suspensor cells in WT and their absence in (**a**). (**b**) a Pa *ESP*-RNAi line. Note also the presence of a single dying cell (arrow) at the basal pole of the suspensor-like structure in Pa *ESP*-RNAi line. Scale bars, 100 μm.

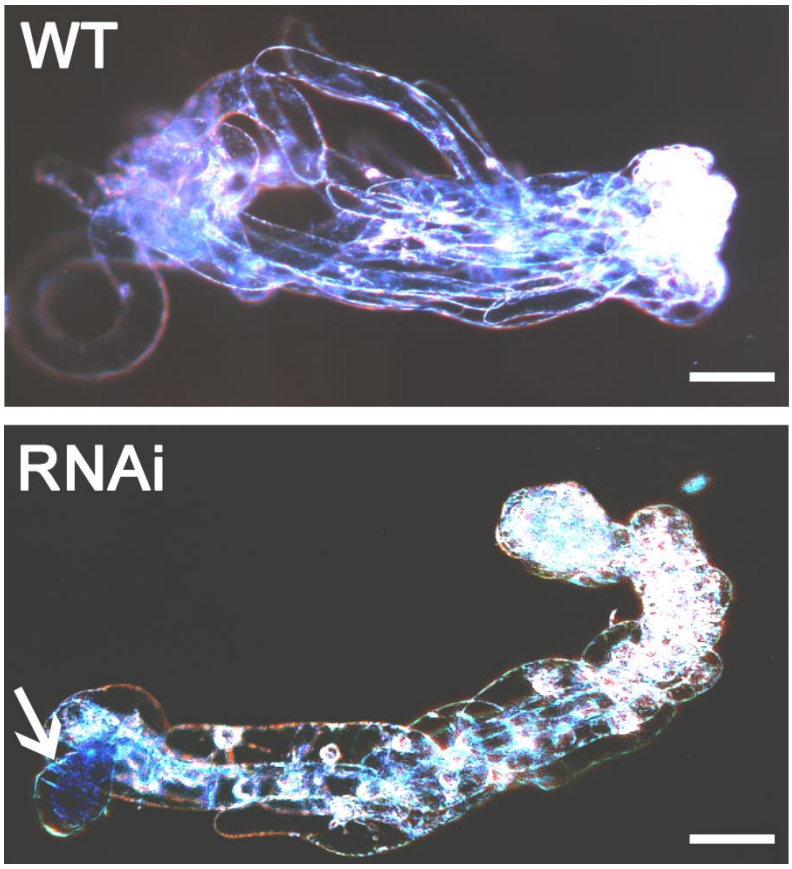

Figure S5

Fig. S6. Pa *ESP* does not complement *rsw4* root swelling phenotype. (**a**) Relative expression levels of Pa *ESP* in WT or *rsw4* lines expressing HA-Pa *ESP* and relative native At *ESP* expression levels in WT or *rsw4* lines expressing HA-Pa ESP. The data show mean ± standard deviation of triplicate experiments with three technical replicates each. Different letters indicate significant differences at $P<0.05$ (n=3; Student's *t*-test).(**b**) Pa *ESP* mRNA to At *ESP* mRNA ratios in WT or *rsw4* lines expressing HA-Pa *ESP*. Absolute quantities of mRNA were calculated using plasmid standards. Notably, mRNA levels of Pa *ESP* are comparable to native At *ESP* levels. The data show mean ± standard deviation of triplicate experiments. Different letters indicate significant differences at $P<0.05$ (n=3; Student's *t*-test). (**c**) Root swelling in *rsw4* lines expressing HA-Pa *ESP*. Plants were exposed to 30°C for 72h as described in Moschou *et al.*, 2013. The data show mean ± standard deviation of triplicate experiments with 10-12 plants each. Different letters indicate significant differences at $P<0.05$ (n=3; Student's *t*-test).

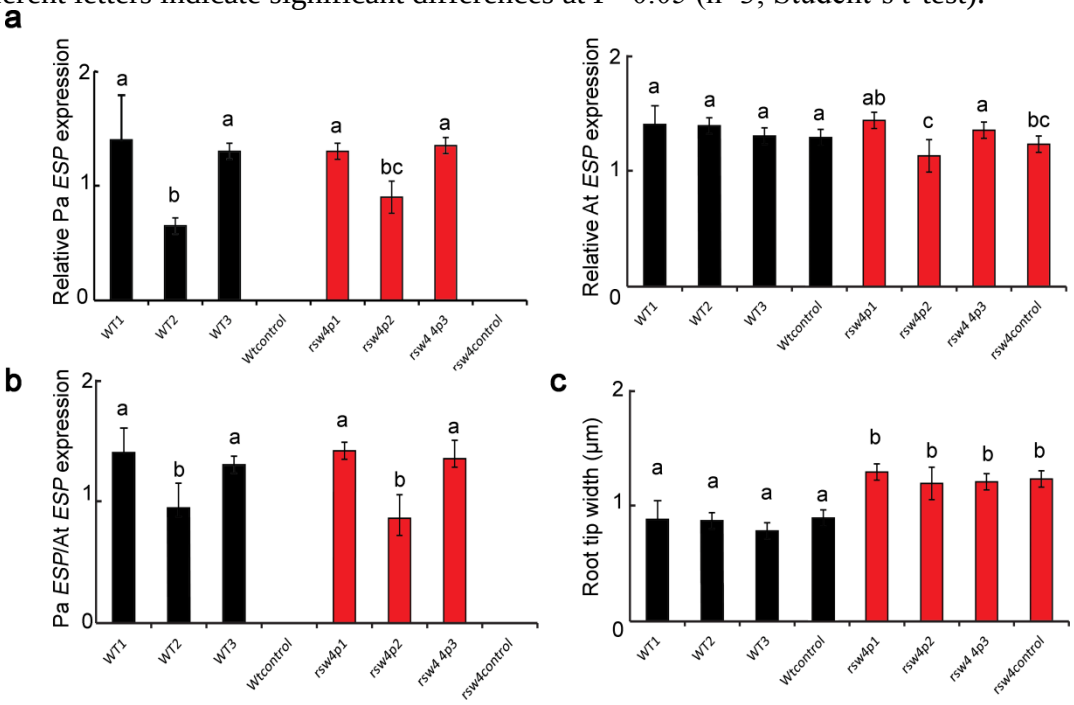

Figure S6

Fig. S7. Effect of inducible Pa *ESP* knockdown on the morphology of cotyledonary embryos.
(**a**) Time course analysis of cotyledonary embryo formation in WT and Pa *ESP*-XVE>RNAi line 5.1. Data are from a single representative experiment, which was repeated twice with similar results. (**b**) Tracking of cotelydonary embryo formation (7-37 days on ABA-containing plates) in WT, Pa *ESP*-RNAi line 4.1 or Pa *ESP*-XVE>RNAi line 5.1. Note that embryos in WT had been formed within 7 days. Scale bars, 5 mm. (**c**) Longitudinal sections of hypocotyls of cotyledonary embryos from WT and Pa *ESP*XVE>RNAi line 5.1. Yellow line demarks meristematic regions. Note the decrease in the size of the meristematic region in Pa *ESP*-XVE>RNAi line. Scale bars, 300 μm.

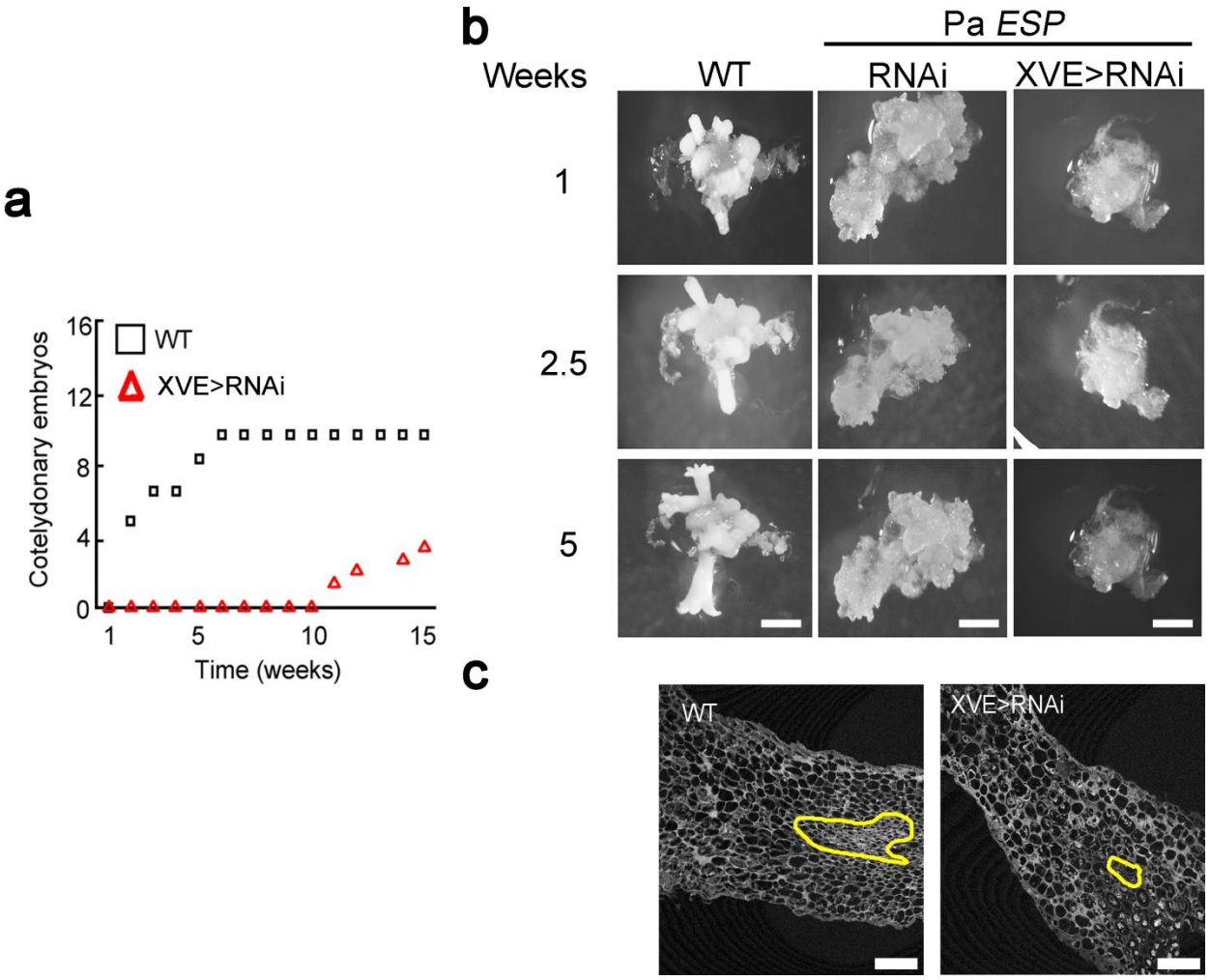

Figure S7

Fig. S8. Width and length of embryos hypocotyl cells, as affected by Pa ESP deficiency. Length and width of embryos hypocotyl cells in Pa *ESP* constitutive (RNAi) or inducible (XVE) lines. The ends of the box indicate the 25-75% quantiles and the vertical line within the box the median. Red whiskers extend from the ends of the box to the outermost data point that falls within the distances computed as follows '3rd quartile + 1.5×(interquartile range)' and '1st quartile - 1.5×(interquartile range)' where 'interquartile range' is the difference between the 1st and 3rd quartiles. If the data points do not reach the computed ranges, then the whiskers are determined by the upper and lower data point values (not including outliers). Blue whiskers indicate the 10% and 90% quartiles. Different values are indicated with black circles (n=20) and data are from a single representative experiment replicated three times. *P* values (comparison to WT) are indicated and were calculated using the non-parametric Wilcoxon test, since values were not normally distributed in the mutants.

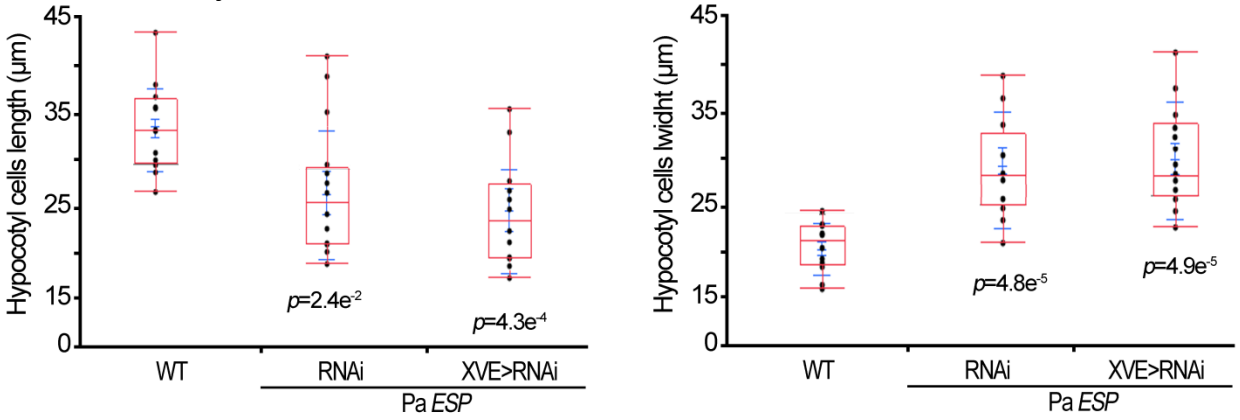

Table S1. List of primers.

Primer name	Primer Sequence (5'->3')	Purpose of use
Separ-RACE3	TGGAAGTGCTTCTTATTGGGAGAACCCTTAGA	PaESP 3'-RACE
Separ-R5-negg	GACCTTCATCGACTGGAACATGAGTTTCCAC	PaESP 5'-RACE
Se-F1	GGTTATCTGAAGGCTTTACTTG	PaESP sequencing
Se-F2	CCTGTTCTTCAGTAAAGGATC	PaESP sequencing
Se-F3	CTGCCATTCAATAATTCTTCTC	PaESP sequencing
Se-R3	CTGAGTGAATAGGACGTTTTATC	PaESP sequencing
Se-F4	TAGCAGTACAACTATTAAGGC	PaESP sequencing
Se-R4	TCACAAAGAACTCCCACCTGC	PaESP sequencing
Se-F5	CTATGGGCACATTAGGCACGC	PaESP sequencing
Se-R5	CCCTTTAATGCTAGTAACTCC	PaESP sequencing
Se-R6	CGTACTTGTCTTTCTCCTTGGC	PaESP sequencing
Separ-AatII-pos	GAAGGACGTCATAACAAGAGTGCAGCAAG	PaESP ORF cloning
Separ-AatII-neg	TTATGACGTCCTTCGAACTGTGATGATG	PaESP ORF cloning
Separ-5-PacI	AATTAATTAATGGATTACAAGGATGACGACGATAAGGAGCCTGCAACTATTCTTGCCAA	PaESP ORF cloning
Separ-3-Sse8387I	AAACCTGCAGGTTAAACAGAAGTTCTCTTAGTTTTAATAG	PaESP ORF cloning
FWPaESPExp1topo	CACCATGGAGCCTGCAACTATTCTTG	PaESP ORF cloning
RvPaESPEXPAscI	TTGGCGCGCCCACGAGATGAAGAAGGAAGAAGCA	PaESP ORF cloning
Sep-C-terminusCHis-P	TTTTAATTAAATGCTCATTGAAAGGGCAGCGTTG	Immunogen preparation
Sep-CHis-M1	ATGATGCCCAACAGAAGTTCTCTTAGTTTTAATAG	Immunogen preparation
Sep-CHis-M2	TTGGCCGGCCTTAATGATGATGATGATGATGCCC	Immunogen preparation
pKOH122-MCS-P	TTGCTAGCTACGTTAATTAAGACGTCGGC	Immunogen preparation
MCS-reverse-SacI	TGACGAGCTCAACAGCTATGACCATGATTACGCC	Immunogen preparation
PaESPRNAiRV1EcoRI	TTGAATTCTCCTTTGGTCTGCTTTCGCC	RNAi lines
FwPaESPRNAiAscI	TTGGCGCGCCCATGGAGCCTGCAACTATTCT	RNAi lines
PaESPRNAiRV2EcoRI	TTGAATTCTCCTTTACTGAAGAACAGGC	RNAi lines
QPaESPF1	TAGTCATTGCAGCGAGTTGG	Q-RT-PCR
QPaESPR1	TGCATGCTCTGAACTTCGTC	Q-RT-PCR
QPaESPF2	GCCAACCTATGGGATGTGAC	Q-RT-PCR
QPaESPR2	CCAACTCGCTGCAATGACTA	Q-RT-PCR
cdc2-ref-F	TCCGACGGGTGCAGAGAA	Q-RT-PCR
cdc2-ref-R	GCTCCATTCAGCCTGATTCAA	Q-RT-PCR
polyUBQ-F	TGGTCGTACTCT GGCGGATTATA	Q-RT-PCR
polyUBQ-R	ACACCTAGCGGCACACAGTTA	Q-RT-PCR
Phosphogluc-ref-F	AATGCAGTTGAAGCCATT CC	Q-RT-PCR
Phosphogluc-ref-R	CCAGTGCCGAAACTCTCTTC	Q-RT-PCR
CYCBL1-F	CACTGCAATGATTCTAGCTTCCA	Q-RT-PCR
CYCBL1-R	GAGCCTGCAGCTTTGAGGAAC	Q-RT-PCR
RBRL-F	TCCCTCAAAGAACTGAGGCTTC	Q-RT-PCR
RBRL-R	CCGTGTGGGACTCGCAAAA	Q-RT-PCR

Method S1. Western blot analysis of Pa ESP protein. Non-cropped western blot image using anti-Pa ESP (mouse 2) of protein extract prepared from WT early embryos (grown for 2 days with PGR). The molecular size marker (Page Ruler Plus Prestained, Fermentas, Sweden) is shown on the right. A chemiluminescence image (anti-Pa ESP) was overlaid with the ladder image obtained by LAS-3000 Luminescent Image Analyzer(Fujifilm, Fuji Photo Film, Germany). Overlay was done in Adobe Photoshop CS6, after color inversion of the ladder image.

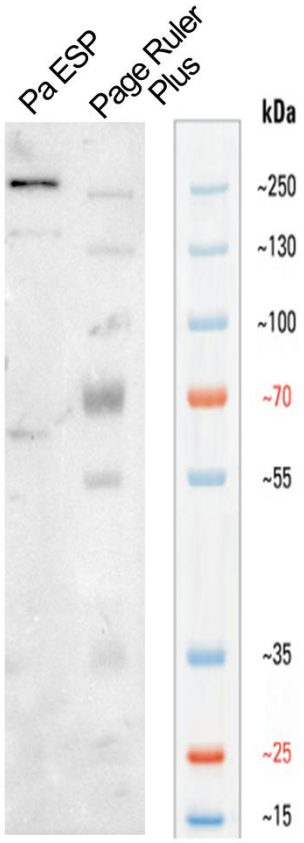

Materials S1

Method S2. SYTOX orange and fluorescein diacetate (FDA) staining was performed on 7-d-old embryo cultures grown without PGR. SYTOX orange and FDA were added to final concentration 1 µM and 2µg/ml, respectively. In some cases we added Evan's blue at a concentration of 0.5% (w/v). After 15 min, the samples were washed twice with −PGR medium on a 50-µm nylon mesh, and samples were examined under an epifluorescence microscope and objectives of 10x with NA=0.45.

Notes S2.Accession numbers.

SpeciesAccession number

Aegilops tauschii GI:475591739Arabidopsis lyrataGI:297799712Arabidopsis thaliana GI:79482708Aspergillus niger GI:145237490Brachypodium distachyon GI:357143740Caenorhabditis elegans GI:17508711Capsella rubella GI:482554895Chlamydomonas reinhardtii GI:159462690Cryptosporidium muris GI:209876352 Cucumis sativus GI:449511406Drosophila melanogaster GI:17647951Ectocarpus siliculosus GI:298714769Galdieria sulphuraria GI:452820916Glycine max GI:356557511Homo sapiens GI:38349532Klebsormidium flaccidum GI:971517283Oryza sativa GI:218191651Ostreococcus lucimarinus GI:145343635Ostreococcus tauri GI:308800150Phaeodactylum tricornutum GI:219125158Physcomitrella patens GI:168012841Phytophthora sojae GI:348688521Picea abies GI:501288956Pinus taedalcl|scaffold498807 on congenie.org.Populus trichocarpa GI:224070579Prunus persica GI:462422597Ricinus communis GI:255576219Saccharomyces cerevisiae GI:398365661Schizosaccharomyces pombe GI:19075403Selaginella moellendorffii GI:302787398Selaginella moellendorffii 2GI:302761250Sorghum bicolor GI:242061008Triticum urartuGI:474396266Vitis vinifera GI:359486090Volvox carteri GI:302847749Zea maysGI:413924384